

Variability of Atmospheric CO₂ Over the Arctic Ocean: Insights From the O-Buoy Chemical Observing Network

K. A. Graham^{1*}, C. D. Holmes^{1*}, G. Friedrich², C. D. Rauschenberg³, C. R. Williams⁴, J. W. Bottenheim^{5†}, F. P. Chavez², J. W. Halfacre⁶, D. K. Perovich^{7*}, P. B. Shepson^{8,9}, W. R. Simpson^{10*}, P. A. Matrai^{3*}

¹Florida State University, Department of Earth, Ocean, and Atmospheric Science, Tallahassee, FL 32306, USA

²Monterey Bay Aquarium Research Institute, Moss Landing, CA 95039, USA

³Bigelow Laboratory for Ocean Sciences, East Boothbay, ME 04544, USA

⁴Cold Regions Research and Engineering Laboratory, Hanover, NH 03755, USA

⁵Environment and Climate Change Canada, Toronto, Ontario M3H 5T4, Canada

⁶University of York, Heslington, York YO10 5DD, United Kingdom

⁷Thayer School of Engineering, Dartmouth College, Hanover, NH 03755, USA

⁸ Purdue University, West Lafayette, IN 47907, USA and ⁹Stony Brook University, Stony Brook, NY 11794, USA

¹⁰University of Alaska, Fairbanks, Fairbanks, AK 99775, USA

Correspondence to KAG (kag16e@my.fsu.edu) and CDH (cdholmes@fsu.edu)

* ORCID – Graham: 0000-0003-2679-3558; Holmes: 0000-0002-2727-0954; Perovich: 0000-0002-0576-0864; Simpson: 0000-0002-8596-7290; Matrai: 0000-0003-1656-5519

† Retired

Key Points:

- Atmospheric CO₂ mixing ratio observations over Arctic Ocean sea ice are examined and interpreted using a chemical transport model
- Seasonal cycle amplitudes of atmospheric CO₂ are smaller, on average, over sea ice than at their coastal counterparts
- Interannual variability of atmospheric CO₂ over sea ice may be impacted by ocean processes, in addition to long-range transport from the mid-latitudes

Abstract

As the Arctic climate rapidly warms, there is a critical need for understanding variability and change in the Arctic carbon cycle, but a lack of long-term observations has hindered progress. This work analyzes and interprets measurements of atmospheric carbon dioxide (CO₂) mixing ratios from long-term on-ice measurements (the O-Buoy Network), as well as coastal observatories from 2009–2016. The on-ice measurements show smaller seasonal amplitudes when compared to the coastal observatories, in contrast to the general observation of poleward increases of seasonal cycle amplitude. Average on-ice mixing ratios were lower than their coastal counterparts during the winter and spring months, contradicting the expectation that wintertime presents a poleward increasing gradient of CO₂. We compare the observations to CO₂ simulated in an updated version of the GEOS-Chem 3-D chemical transport model, which includes new tracers of air mass history and CO₂ sources and sinks. The model reproduces the observed features of the seasonal cycle and shows that terrestrial biosphere fluxes and synoptic transport explain most CO₂ variability over the surface of the Arctic Ocean. Interannually, the coastal observations were more comparable in overall CO₂ growth than concurrent measurements over sea ice. We find evidence indicating the presence of ocean gas exchange in and around sea ice during periods where this growth discrepancy occurs. Periods with large spatial gradients are examined, showing that release of CO₂ from Arctic waters in years with low sea ice concentration could possibly contribute to the greater interannual increase of CO₂ over sea ice compared to land.

Plain Language Summary

The Arctic is undergoing immense biogeochemical change, due to the enhanced warming it has experienced in recent decades. These rapid changes contribute to uncertainty in the Arctic carbon cycle and the physical processes impacting carbon gas exchange at these latitudes. In this work, we analyzed and modeled atmospheric CO₂ concentrations obtained over Arctic sea ice and compared them with CO₂ concentrations measured at coastal observatories. We found that CO₂ concentrations over sea ice do not follow the general observed behavior that seasonal cycle amplitudes of CO₂ (dominated by photosynthesis and respiration of the terrestrial biosphere) are increasing poleward as our global climate continues to warm. We also found that the interannual growth of CO₂ is different between the coast and over sea ice. Our findings suggest that another physical process (likely gas exchange in and around sea ice) may be impacting atmospheric CO₂ concentrations year-to-year at the highest latitudes and obtaining more observations over sea ice will add to knowledge of this sparsely observed region.

1 Introduction

There is no region on Earth where climate change is happening faster than the Arctic, where temperatures are increasing at twice the global average rate (Osborne et al., 2018). This rapid environmental change has made quantifying the carbon budget at the northern high latitudes difficult. In particular, assessing whether the Arctic will behave as a carbon source or

sink in the coming decades remains a challenging task (McGuire et al., 2009, 2010). Since atmospheric CO₂ mixing ratios are a function of meteorological patterns (transport and vertical mixing) and exchange with the surface (fluxes), quantifying CO₂ mixing ratios and variability will provide metrics that increase our understanding of processes impacting the carbon cycle at high latitudes.

Observations have already shown that large carbon reservoirs in the Arctic are changing (McGuire et al., 2014). The uptake and release of carbon by the terrestrial biosphere dominates the seasonal cycle of atmospheric CO₂ mixing ratios over land north of 45 °N, especially in the summertime (Keeling et al., 1996). The boreal terrestrial biosphere is a net carbon sink (Pan et al., 2011); furthermore, it has previously been shown that warmer surface air temperatures are lengthening the growing season (Myneni et al., 1997), resulting in increased seasonal amplitudes of atmospheric CO₂ (Graven et al., 2013). However, this terrestrial biological response to warming and other climatic changes may be heterogeneous and non-linear (Soja et al., 2007), due to the variations in plant species composition across boreal ecosystems (Goetz et al., 2005) and their migration in response to climate change (Elmendorf et al., 2012). Studies have also shown climatic variables, like air temperature and snow-cover, impact the interannual variability of CO₂ fluxes at high latitudes (Rennermalm et al., 2005; Groendahl et al., 2007). In addition, disturbances like insect or disease infestation (Verbyla, 2008), fires (Kasischke et al., 2010), and anthropogenic impacts (Magnani et al., 2007) further contribute to the difficulty of quantifying the carbon cycle and CO₂ exchange at the northern high latitudes.

The global ocean is a net sink for atmospheric CO₂. Arctic Ocean uptake has been estimated at $180 \pm 130 \text{ Tg C yr}^{-1}$, which is $8 \pm 6 \%$ of global ocean CO₂ uptake (Ciais et al., 2013; Takahashi, 2002; Takahashi et al., 2009; Yasunaka et al., 2018) while the Arctic Ocean covers just 4 % of global ocean surface area. In ice-free regions, high-latitude oceans are seasonally strong CO₂ sinks due to fast gas exchange under high winds, high gas solubility at cold temperatures, and high CO₂ uptake by primary production in nutrient-rich waters (Takahashi et al., 2009). The uptake of CO₂ by sea-ice covered areas, however, has been traditionally considered to be minimal or non-existent, though this view is changing (Loose et al., 2011; Miller et al., 2011). Loss of sea ice may enhance air to sea fluxes of CO₂ (Bates et al., 2006). The effects of these observed changes in sea ice on the Arctic carbon cycle are highly uncertain for the rest of the century (Cai et al., 2010; McGuire et al., 2009, 2010).

Understanding the behavior of CO₂ over the Arctic Ocean has been limited by the availability of long-term measurements. The harsh polar sea ice conditions of the Arctic Ocean make obtaining observations difficult, especially for autonomous sensors. Most long-term Arctic atmospheric observations, particularly chemical composition data, have been collected at terrestrial stations around the periphery of the Arctic Ocean. This results in a major spatial gap in surface data collection. Measurements of CO₂ mixing ratios and fluxes over sea ice have been made from research vessels, such as icebreakers, that may alter atmosphere-ocean fluxes by breaking ice and exposing the underlying seawater, or from ice camps that preferentially sample certain seasons and ice conditions (mainly spring melt and fall freeze-up seasons) (Else et al.,

2011; Geilfus et al., 2012, 2015; Miller et al., 2011; Nomura et al., 2013; Prytherch et al., 2017; Semiletov et al., 2004). Additionally, the Arctic Ocean has been observed to be regionally complex. It is currently described as a strong CO₂ sink in the Chukchi Sea (Bates et al., 2006), the East Siberian Sea (Semiletov et al., 2007), and pan-Arctic (Yasunaka et al., 2016, 2018), especially in open water regions, but a CO₂ source nearshore (Semiletov et al., 2007; Williams & Carmack, 2015), and neutral in the Canada Basin (Cai et al., 2010).

This work presents a new, multi-year record of atmospheric CO₂ mixing ratios directly measured by autonomous, ice-tethered buoys in the Arctic Ocean. The O-Buoy Network measured atmospheric CO₂ mixing ratios from 2009–2016, and provides the longest, most extensive collection of in situ CO₂ observations collected over sea ice. In this work, we examine the seasonal and interannual variability in the observations, and further interpret them using an atmospheric CO₂ transport model. We discuss the differences in observed quantities between coastal and on-ice locations, as well as the physical processes that control atmospheric CO₂ mixing ratios in the Arctic.

2 Methods

2.1 O-Buoy CO₂ measurements

The O-Buoy Network of Chemical Sensors (O-Buoys) is a set of ice-tethered, autonomous buoys deployed in the Arctic Ocean to measure atmospheric trace gases, including CO₂ and meteorological variables (Knepp et al., 2010). Thirteen overlapping deployments occurred during 2009–2016, operating for as long as 16 months (Fig. 1, Table S1). O-Buoys were deployed at latitudes between 76 °N and 89 °N and most remained north of 75 °N for the duration of their deployments. Nine O-Buoys were deployed in the Beaufort Gyre, two in the East Siberian Sea, and two in the central Arctic Ocean near the North Pole eventually drifting through Fram Strait.

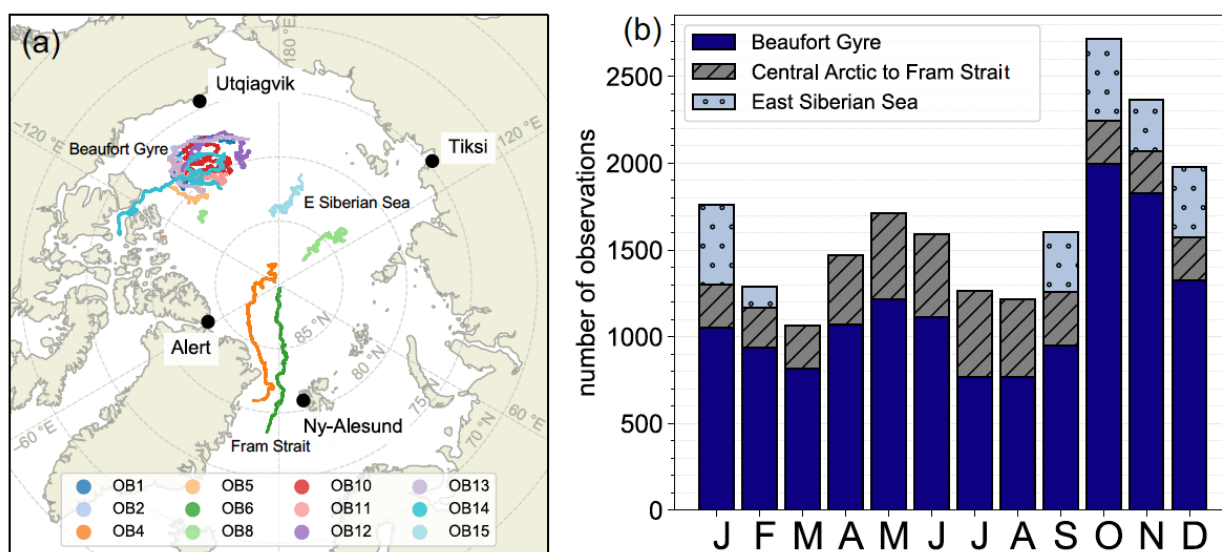


Figure 1. (a) Drift trajectories of O-Buoys (OB) measuring CO₂ (2009–2016) and coastal stations with CO₂ measurements used in this work. (b) Number of CO₂ observations obtained by the O-Buoys in each month, divided into regions where the measurements were obtained.

Each O-Buoy measured ambient atmospheric CO₂ mixing ratios every 3 hours with a nondispersive infrared analyzer adapted for buoy deployment (modified LI-COR 820). Meteorological observations on the O-Buoys included wind speed and direction (RM Young Model 05103), humidity and temperature (Vaisala HMP45C), and pressure (Vaisala PTB110), and were reported hourly. Measurements of ozone by absorption-based ozone monitors and the reactive gas bromine monoxide (BrO) by multi-axis optical absorption spectroscopy have been reported separately (Burd et al., 2017; Halfacre et al., 2014; Peterson et al., 2016; Swanson et al., 2020). Knepp et al. (2010) provide further details of the O-Buoy design and instrument performance characteristics. Measurements of ambient atmospheric CO₂ were regularly calibrated in the field with two gas cylinders containing known standards installed in the O-Buoy hull, whose CO₂ mole fraction in dry air was measured with high precision and accuracy prior to deployment. The uncertainties in the in-buoy calibration gases themselves were determined prior to each long-term O-Buoy deployment. When possible, calibrations were repeated at the end of the deployments. At deployment, the CO₂ measurements had a precision of ± 0.1 ppm and accuracy of ± 0.2 ppm, sufficient to monitor the seasonal variations of 25–30 ppm against atmospheric background mixing ratios around 400 ppm, as well as day-to-day variability of up to ± 7 ppm. This accuracy is comparable to pairs of samples collected by the NOAA ESRL across their observation network (NOAA ESRL Global Monitoring Division, 2015; Zhao & Tans, 2006). Post-deployment corrections to the CO₂ mixing ratios were done when a multi-parameter (CO₂, temperature, relative humidity and atmospheric pressure, with in-sensor and environmental values for each parameter) analysis of the calibration gases indicated a residual was related to the internal pressure of the CO₂ sensor. This correction was less than 5 % of the measured value and only used in a few deployments. For further information, refer to Knepp et al. (2010).

2.2 Coastal sampling stations CO₂ measurements

To provide a more complete representation of CO₂ variability around the Arctic Ocean, we examined measurements at Arctic coastal sites from the CO₂ GLOBALVIEWplus v4.0 ObsPack (Cooperative Global Atmospheric Data Integration Project, 2018). The Arctic sites (<https://www.esrl.noaa.gov/gmd/dv/site/>) are at Alert, Nunavut, Canada (ALT), Utqiagvik, Alaska, USA (BRW), Ny-Alesund, Svalbard, Norway (ZEP), and Tiksi, Russia (TIK) (Fig. 1a). The stations are operated by Environment Canada (ALT), U.S. NOAA (BRW), the Norwegian Institute for Air Research (ZEP), and U.S. NOAA/ Russian Federation's Roshydromet/ U.S. NSF/ Finnish Meteorological Institute (TIK). Observations were conducted using discrete flask samples, which are normally collected weekly in 2–4 replicate flasks. For some analyses, we used hourly in situ CO₂ mixing ratios at Utqiagvik, AK, also from GLOBALVIEWplus.

CO₂ flask samples were collected when winds were within a designated clean air sector (e.g. 0 to 90 °E at Utqiagvik) and exceeded 2 m s⁻¹, both of which minimized the likelihood of contamination from local anthropogenic CO₂ sources. All flask samples were collected in pairs, with the mixing ratio differences between pair members lying within 0.5 ppm of each other

(Dlugokencky et al., 2016). We removed three outlier measurements at Alert, NU, because they differed from preceding and following observations by more than 10 ppm: 2014–01–02 19Z, 2014–01–30 20Z, and 2014–02–26 19Z. Similarly, we removed the following six outliers at Utqiagvik, AK: 2009–08–31 10Z, 2009–02–27 14Z, 2010–11–26 15Z, 2015–10–02 18Z, 2015–10–05 18Z, 2016–12–13 23Z. For times when multiple CO₂ observations were recorded at one location, we averaged the measurements made in the same hour. We set the measurement times at the coastal stations to the nearest hour to identify measurements that are nearly simultaneous with the O-Buoys.

2.3 Sea ice concentration and thickness

To understand the sea ice environment around the O-Buoys, we used sea ice concentration (unitless fraction varying 0–1) from passive microwave remote sensing (Nimbus-7 SMMR and DMSP SSM/I-SSMIS Passive Microwave Data, Version 1, available from the National Snow and Ice Data Center, <https://nsidc.org/data/nsidc-0051>). Data are generated from brightness temperature measurements and are designed to provide a continuous time series of sea ice concentrations spanning the coverage of several passive microwave instruments. The data are provided in a polar stereographic projection at a grid cell size of 25×25 km, and the pixel with each O-Buoy was selected.

2.4 GEOS-Chem atmospheric transport model

We simulated atmospheric CO₂ mixing ratios and diagnosed atmospheric transport using the GEOS-Chem global 3-D chemical transport model (version 12.7.2, www.geos-chem.org). The model was driven by assimilated meteorology from the NASA Modern-Era Retrospective analysis for Research and Applications, Version 2 (MERRA-2; Gelaro et al., 2017) and simulations here have a resolution of $2^\circ \times 2.5^\circ$ with 47 vertical levels. Model results cover the complete O-Buoy period from 2009–2016 with hourly sampling at the locations of the O-Buoys and coastal stations.

Since the CO₂ simulation relies on the accuracy of the meteorological data and because there are few surface observations available to assimilate in the Arctic, we evaluated MERRA-2 over the Arctic Ocean against O-Buoy meteorological measurements. We compared MERRA-2 at its native horizontal resolution ($0.5^\circ \times 0.625^\circ$) and at the resolution used in the simulations here ($2^\circ \times 2.5^\circ$) to measurements of sea-level pressure, air temperature, and wind speed on O-Buoys 11 and 12. Supplementary Table 2 provides full results of the comparisons for sea-level pressure, air temperature, and wind speed. The coefficient of determination (R^2) for sea-level pressure and air temperature shows a close relationship between observed and reanalysis quantities (at $2^\circ \times 2.5^\circ$, sea-level pressure $R^2 = 0.983$ and RMSE = 1.27 hPa; air temperature $R^2 = 0.977$ and RMSE = 2.47 K; Supplementary Table 2). For wind speed, the apparently poor comparison (at $2^\circ \times 2.5^\circ$, $R^2 = 0.558$ and RMSE = 2.12 m s^{-1}) may be due to occasional rime-icing of the O-Buoy anemometer. Since large-scale atmospheric transport is controlled by synoptic pressure gradients, our surface pressure comparison suggests a reasonable

representation of long-range transport. In addition, prior GEOS-Chem work using GEOS-5 derived meteorology also supports the reanalysis' ability to resolve long-range transport events in the Arctic (Fisher et al., 2010; Wang et al., 2011).

2.4.1 CO₂ simulation and CO₂ source tags

The GEOS-Chem CO₂ simulation was previously described by Nassar et al. (2010). For this work, all emissions and surface fluxes were updated, using inventories summarized in Table 1. Anthropogenic emissions are from the Community Emissions Data System (CEDS; Hoesly et al., 2018). The CEDS inventory ended in 2014, so our 2015 and 2016 emissions consist of the 2014 CEDS spatial pattern scaled to match the global total emissions for those later years in the Open-Source Data Inventory for Anthropogenic Carbon Dioxide (ODIAC; Oda & Maksyutov, 2011). We used this approach, rather than using ODIAC alone, because the CEDS inventory includes anthropogenic biofuel emissions that are not in ODIAC. Biomass burning emissions came from the Global Fire Emissions Database (GFED4.1s; van der Werf et al., 2017). Net terrestrial and ocean fluxes were taken from NOAA CarbonTracker (version CT2019; Jacobson et al., 2020, with updates documented at carbontracker.noaa.gov). Similar to other flux inversions, CarbonTracker provides no estimate of CO₂ fluxes over the Arctic Ocean, which is equivalent to assuming zero flux. Therefore, the analysis in Section 3 critically examines if surface CO₂ fluxes over the Arctic Ocean are necessary to explain the O-Buoy CO₂ measurements. Atmospheric chemical production of CO₂ from oxidation of CO and organic gases was archived from a prior GEOS-Chem simulation (Bukosa et al., 2021).

The CO₂ simulation was initialized in January 2007 with the observed global marine surface mean CO₂ mixing ratio (382.8 ppm; Dlugokencky and Tans, NOAA/GML, www.esrl.noaa.gov/gmd/ccgg/trends/, accessed 2020–12–15) and the CO₂ spatial distribution from a prior CO₂ simulation by Nassar et al. (2010). After two years of model spin up, results were analyzed beginning in 2009 and continuing through 2016.

To understand the fluxes that contributed to total CO₂ mixing ratios in the model, we tagged CO₂ from each source and sink for the duration of the simulation (2007–2016). The six tags included fossil fuel emissions, biomass burning emissions, net ocean flux, net terrestrial biosphere flux, chemical production of CO₂, and initial condition (each corresponding with the datasets described in Table 1). At every time and location simulated, the sum of the CO₂ tags equaled the total modeled CO₂ mixing ratios, within some small numerical error.

As detailed in Table 1, the global carbon budget in the simulation for 2014 included anthropogenic emissions to the atmosphere of 9.7 Pg C yr⁻¹. Atmospheric chemistry and biomass burning added another 1.0 and 0.4 Pg C yr⁻¹, respectively. Terrestrial and ocean fluxes can be positive or negative, depending on location and season, but in the net were 5.3 Pg C yr⁻¹ uptake to the land and 3.2 Pg C yr⁻¹ uptake to the ocean. Therefore, the atmospheric accumulation was 2.6 Pg C yr⁻¹ in 2014. Flux inventories varied from year to year in the simulation, but the 2014 budget is similar to other simulated years. The total carbon budget in our model generally aligns with recent estimates from the Global Carbon Project (GCP; Friedlingstein et al., 2019). In the

246 GCP synthesis for 2014, human-induced emissions equaled 9.6 ± 0.5 Pg C yr⁻¹, land use change
 247 emissions totaled 1.7 ± 0.7 Pg C yr⁻¹, and land and ocean uptake equaled 3.7 ± 0.9 Pg C yr⁻¹ and
 248 2.6 ± 0.5 Pg C yr⁻¹, respectively. The atmospheric growth rate was estimated to be 4.3 ± 0.2 Pg
 249 C yr⁻¹; the unaccounted imbalance of the carbon budget was 0.7 Pg C yr⁻¹ (Friedlingstein et al.,
 250 2019).

Table 1: Budget of atmospheric CO₂ sources and sinks in GEOS-Chem.

Source or sink	Global annual flux total (2014) ^a [Pg C yr ⁻¹]	Inventory	Reference
Anthropogenic ^{b,c}	9.7	CEDS	Hoesly et al. (2018)
Land ^d	-5.3	CarbonTracker 2019	Jacobsen et al. (2020)
Ocean ^d	-3.2	CarbonTracker 2019	Jacobsen et al. (2020)
Biomass burning ^c	0.4	GFED4.1s	van der Werf et al. (2017)
Atmospheric chemistry ^{c,e}	1.0	GEOS-Chem	Bukosa et al. (2021)

^a Positive flux values increase atmospheric CO₂. All flux inventories used in the model vary by year and values for 2014 are provided here.

^b Includes fossil fuel, biofuel, agriculture, and industrial sources. The CEDS inventory ends in 2014. The 2015 and 2016 anthropogenic emissions in this work are computed by scaling the CEDS 2014 pattern to the global total emissions reported by ODIAC (Oda et al., 2010).

^c Monthly temporal resolution

^d 3-hourly temporal resolution.

^e Atmospheric chemical production of CO₂ from the oxidation of other carbon gases (CO and volatile organic compounds) is archived from a previous full chemistry simulation in GEOS-Chem.

2.4.2 Atmospheric transport diagnostic tracers

We defined new tracers of atmospheric transport to help interpret differences in CO₂ between Arctic sites. The tracers quantify airmass contact with different surface types: sea ice, open water, and land. The sea ice locations and fractions vary in time, as specified by MERRA-2, while others are temporally constant. Over each of these surfaces the tracers were emitted at a uniform rate of 1 molecule m⁻² s⁻¹. The tracers were subsequently transported identically to CO₂ and decayed with a specified e-fold lifetime. The tracers are similar to e90 (an artificial tracer with 90-day decay time; Prather et al., 2011), but resolve contact with different surface types whereas e90 reflects overall surface contact. The tracer surface contact sum (TSCS; the sum of each tracer emitted over each surface type) allows us to understand total surface contact and vertical transport. A greater TSCS at the surface indicates “trapped” air within the boundary layer (i.e., less free tropospheric entrainment), whereas a lower TSCS at the surface indicates greater mixing and ventilation.

This paper discusses surface contact tracers with 5-day lifetimes, but we also tested additional lifetimes up to 90 days. The atmospheric tracer values were then sampled at the times and locations of the observed CO₂ measurements, to provide insight into upwind surfaces potentially influencing the observed CO₂ mixing ratios over the timescale of the imposed

lifetime. The analysis focuses on spatial and temporal variations in the surface contact tracers, which reflect differences in the upwind contact of air masses with the different surface types. Absolute magnitudes of the contact tracer mixing ratios, by contrast, are not as meaningful because they are proportional to an arbitrary choice of surface emission rate ($1 \text{ molecule m}^{-2} \text{ s}^{-1}$).

2.5 Statistical methods

Several statistical analyses were used to quantify seasonal cycles, day-to-day variability, growth rates, and spatial differences in CO_2 measurements. These methods account for the different sampling frequencies and duration of measurements at the various O-Buoys and coastal stations.

For each O-Buoy and coastal station in both observations and model prediction, we quantified multi-year CO_2 growth rates with ordinary least squares regression separately for the months of April–May (CO_2 maximum) and August–September (CO_2 minimum).

We followed the NOAA ESRL method (with code obtained from <https://www.esrl.noaa.gov/gmd/ccgg/mb/mbfit/mbfit.html>) described by Thoning et al. (1989) to calculate smoothed curves of CO_2 measurements and an overall reference trend at Utqiagvik, AK (using flask and in situ measurements). The smoothed curve of a time series of CO_2 measurements is defined as the function fit plus the filtered residuals using a short-term cutoff value of 80 days. The trend is defined as the upward growth in the data with the seasonal cycle removed. It is the polynomial part of the function fit plus the filtered residuals using the long-term cutoff value (667-day cutoff frequency). To aid in overall time series analysis, we detrended the CO_2 time series for all O-Buoys and coastal stations using this common trend from Utqiagvik, AK (Fig. S1). In addition, we subtract the smoothed data from our series of CO_2 measurements to obtain a time series of the high-frequency variability in our dataset, from which we calculated the mean standard deviation per month. For Utqiagvik, AK, we calculated the standard deviation from both the in situ and flask data, resampled to the same frequency as the O-Buoy period. Similarly, this method was followed for calculating Pearson correlation coefficient values between the observed and modeled CO_2 mixing ratios, as well as the observed CO_2 mixing ratios and observed sea ice concentrations.

O-Buoy CO_2 records are not continuous due to deployment timing, destruction of O-Buoys, or instrumental problems. To compare seasonal amplitudes between the coastal stations and O-Buoys, we compared years where O-Buoy observations were continuous for an entire seasonal cycle (2011, 2012, 2015, 2016). From each time series, we removed the trend calculated at Utqiagvik, AK. Then, seasonal amplitudes were calculated as the maximum daily mean CO_2 minus minimum daily mean in each year. We also explored seasonal amplitudes calculated from a 7-day rolling mean. Deployments prior to 2011 did not provide sufficient samples in the spring and summer to estimate a seasonal amplitude.

For case studies of differences between O-Buoys and coastal stations, we compared daily means of CO_2 mixing ratio, with variance calculated as the unbiased squared standard deviation. If two O-Buoys co-observed, their measurements were averaged together daily.

3 Results and discussion

The O-Buoy network provides a wealth of data on atmospheric CO₂ mixing ratios and variability over the sparsely observed Arctic Ocean on time scales from hours to years. Figure 1 shows the spatial and temporal coverage of the data. The 13 O-Buoys measured CO₂ and meteorological observations for a total of 1,873 unique dates during 2009–2016, obtaining data for 17,116 cumulative hours. The longest of the O-Buoy deployments with CO₂ observations lasted 13 months and drifted over 4,750 kilometers (O-Buoy 14). Measurements span the entire annual cycle (Fig. 1b). Since the O-Buoys were most commonly deployed in August–October, the months of October–December are sampled most intensively (over 2,000 measurements each month in the total dataset), but there are at least 1,000 measurements in every month. Regionally, the Beaufort Gyre has the largest fraction of O-Buoy CO₂ measurements (69%), followed by the central Arctic through Fram Strait (20%) and the East Siberian Sea (11%) (Fig. 1b).

The O-Buoys were deployed during times of varying sea ice cover, which has changed extensively in recent decades. In addition to declining summertime minima, multi-year sea ice constitutes a smaller fraction of the remaining sea ice. Partially open waters, melt ponds, leads, or cracks may provide opportunities for both atmospheric CO₂ enhancement and decrease. If other environmental processes remained constant, an increased oceanic CO₂ uptake capacity should result in a lower atmospheric CO₂ growth rate. An ongoing debate on whether the seasonally opening central Arctic Ocean waters are capable of absorbing more atmospheric CO₂ (Bates et al., 2006; Cai et al., 2010; Else et al., 2013; Jutterström & Anderson, 2010) appears to lean towards a weak sink (relatively weak due to low biological activity and increasing

Table 2: CO₂ seasonal cycle amplitudes (ppm) in observations and the GEOS-Chem model^a. Observed trend at Utqiagvik calculated and removed from all series.

Location	Data Type	Averaging	2011	2012	2015	2016	Mean
Utqiagvik, AK	Flask + in situ	Daily	26.9	25.4	25.1	22.5	25.0 ± 1.6
	Model	Daily	28.8	37.4	30.5	30.1	31.7 ± 3.4
	Flask + in situ	7-day	23.2	21.8	20.3	20.5	21.4 ± 1.2
	Model	7-day	26.3	30.4	22.9	25.1	26.2 ± 2.7
Alert, NU ^b	Flask	Daily	22.9	20.2	19.7	19.3	20.5 ± 1.4
	Model	Daily	24.9	27.7	23.8	24.8	25.3 ± 1.5
O-Buoys	In situ	Daily	22.8	19.7	20.4	26.1	22.2 ± 2.5
	Model	Daily	31.1	29.5	25.2	27.8	28.4 ± 2.2
	In situ	7-day	20.9	18.8	18.7	24.5	20.7 ± 2.3
	Model	7-day	27.0	27.5	22.4	24.2	25.3 ± 2.1

^a Amplitudes are calculated from the maximum value minus minimum value within a year, using both daily mean values and 7-day rolling mean values. The model was resampled to match the frequency of observed measurements.

^b Only flask data was considered from the NOAA GLOBALVIEW+ ObsPack at Alert, NU.

stratification; i.e., a lower seasonal CO₂ growth rate). At times, a weak source of CO₂ has been estimated for Pacific-influenced coastal Arctic seas, due to increasing ventilation and a higher seasonal CO₂ growth rate (Cai et al., 2014).

3.1 CO₂ Seasonality

We find that atmospheric CO₂ mixing ratios measured by O-Buoys over the remote ice-covered Arctic Ocean generally have similar seasonal cycles and growth as compared to mixing ratios measured along Arctic coasts, with some notable differences (Fig. 2a). Table 2 shows that the average CO₂ seasonal cycle amplitude over the Arctic Ocean (22.2 ± 2.5 ppm, mean \pm standard deviation) was slightly smaller than at Utqiagvik, AK (25.0 ± 1.6 ppm) and larger than at Alert, NU (20.5 ± 1.4 ppm) during the period from 2011–2016. These relative differences are observed in 3 of the 4 years. In 3 years, we also find that the peak CO₂ mixing ratios in winter are smaller over sea ice at the O-Buoys than at the surrounding Arctic coastal stations (i.e., 2012, 2014, 2015; Fig. 2). From past literature, it is generally expected that the atmospheric CO₂ maxima in winter increase poleward, and that the seasonal cycle amplitude also increases poleward (Graven et al., 2013; Ramanathan et al., 1979; Tans et al., 1990). O-Buoy data show that both of these large-scale atmospheric patterns stop or reverse when progressing northward from Utqiagvik, AK (71.3 °N) to over the Arctic Ocean.

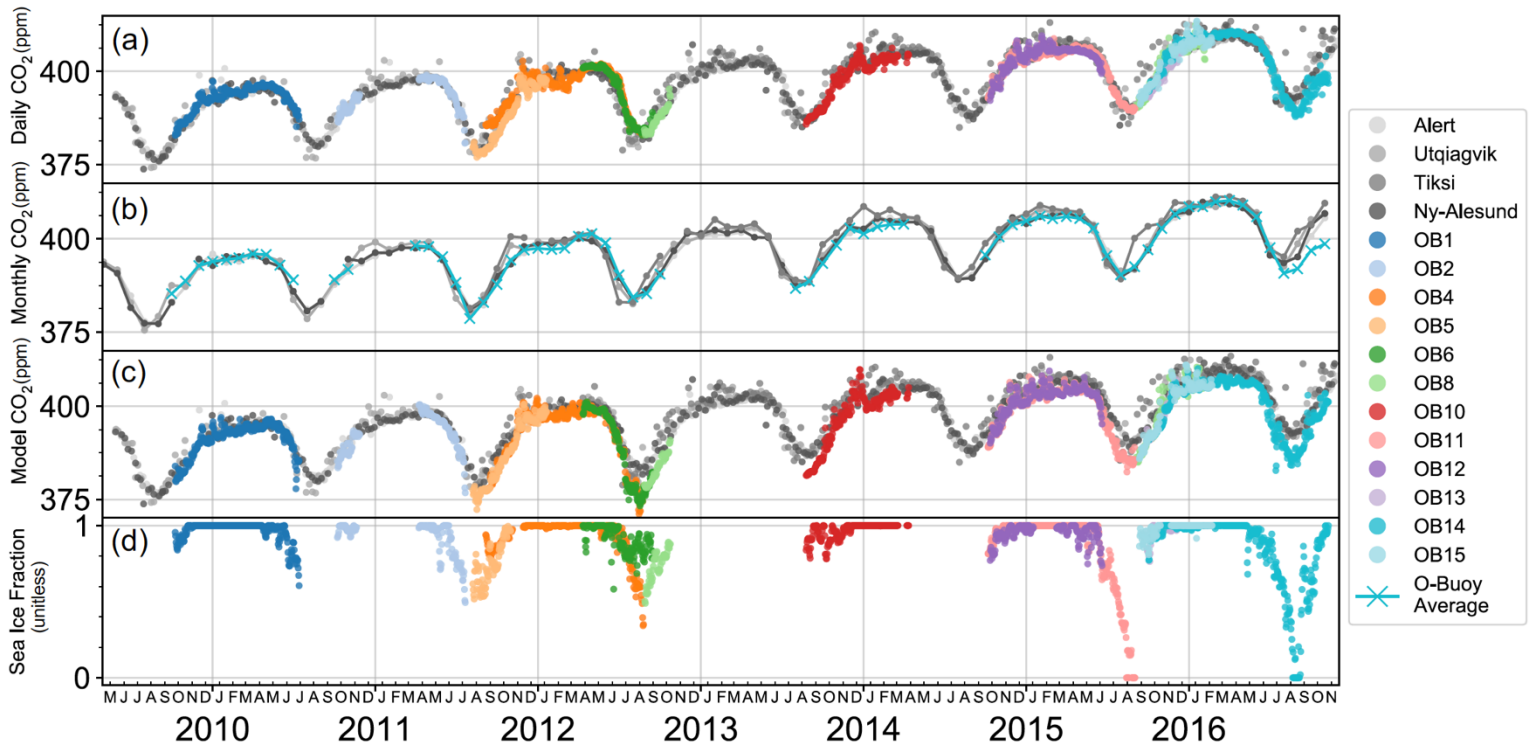


Figure 2. Daily (a) and monthly (b) mean CO₂ mixing ratios observed over the Arctic Ocean from the O-Buoys and at coastal Arctic stations. (c) Daily mean CO₂ simulated at the O-Buoy and coastal locations. (d) Daily sea ice concentrations observed at the O-Buoys.

The mean CO₂ seasonal cycle amplitudes over the Arctic Ocean and coastal sites during 2011–2016 (19–24 ppm) are all greater than the average amplitude measured at Utqiagvik, AK over its entire record (16.6 ± 1.8 ppm for 1973–2015; NOAA). These results are consistent with an increasing seasonal amplitude in the high northern latitudes over the last several decades (Graven et al., 2013), which has grown up to 50 % north of 45 °N since 1960 (Bacastow et al., 1985; Graven et al., 2013; Keeling et al., 1996; Randerson et al., 1997). This increasing seasonal amplitude has been attributed to the combined effect of changes in Arctic and boreal terrestrial vegetation dynamics (i.e., increased vegetation cover, longer and greater gross primary production) and climate change (i.e., warmer air temperature and increased precipitation) (Forkel et al., 2016), both favoring earlier and longer CO₂ uptake (Reichstein et al., 2007). In addition, it has been argued that the changes in boreal land fluxes are driven mostly by photosynthesis and respiration processes rather than agriculture and land use change, plant phenology, fire, and permafrost dynamics (Graven et al., 2013; Reichstein et al., 2007).

Figure 2c shows simulated CO₂ mixing ratios in GEOS-Chem compared to observations at the O-Buoys and Arctic coastal stations (Fig. 2a). The model is sufficiently similar to observations that differences are difficult to discern in Figure 2, so monthly mean model error is shown in Figure 3. Simulated CO₂ is generally within 1 ppm of the observations during winter, and within 5 ppm of the observations in summer. Table 2 also shows the amplitude of the simulated seasonal cycle. While the model’s seasonal cycle amplitude is 25–30 % larger than observations at all Arctic sites for reasons to be discussed in Section 3.3, the model nevertheless predicts the same relative differences in the amplitude between sites: decreasing CO₂ amplitude from Utqiagvik, AK (31.7 ± 3.4 ppm) to the O-Buoys (28.4 ± 2.2 ppm) to Alert, NU (25.3 ± 1.5 ppm). Likewise, the model also correctly predicts that peak wintertime CO₂ mixing ratios at the buoys are the same or smaller than at Utqiagvik (Fig. 2). Over two-thirds of the O-Buoy measurements were recorded in the Beaufort Gyre (Fig. 1), less than 1000 km away from Utqiagvik, AK, so the CO₂ amplitude and peak drop relatively quickly when moving offshore into the Arctic Ocean.

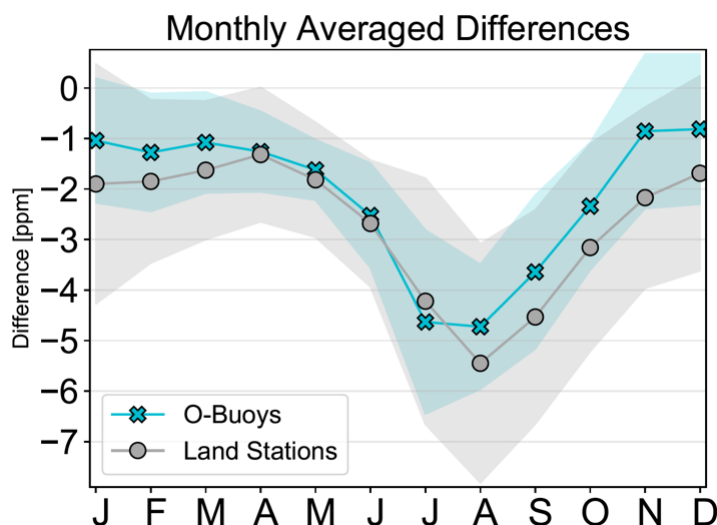


Figure 3. GEOS-Chem CO₂ model error (model minus observation) averaged monthly for all land stations and O-Buoys, with standard deviation shaded.

372 We use the model to understand the combination of marine, terrestrial, and transport
 373 processes that drive the smaller CO₂ seasonal cycle amplitude and smaller peak winter CO₂ over
 374 the Arctic Ocean. Relevant ocean processes could include winter uptake of atmospheric CO₂
 375 through leads or sea ice over undersaturated water (Miller et al., 2011) or summertime gas
 376 exchange through leads, melt ponds, or sea ice (Loose et al., 2011). While respiration in the
 377 terrestrial biosphere is the general cause of high atmospheric CO₂ in winter, the polar dome
 378 airmass may partially isolate O-Buoys and Alert, NU from this CO₂ source, giving these sites
 379 lower winter CO₂ (Bozem et al., 2019; Serreze and Barry, 2014). As already described, the
 380 GEOS-Chem model correctly predicts the smaller observed CO₂ amplitude and winter peak over
 381 the Arctic Ocean and at Alert, NU than at Utqiagvik, AK. Within the model, these features
 382 cannot be driven by CO₂ fluxes over the Arctic Ocean sea ice because those fluxes are prescribed
 383 to be zero (following CarbonTracker2019). CO₂ tags in the model, shown in Figure 4 for 2014–
 384 2015, demonstrate 90–100 % of the CO₂ seasonal cycle amplitude over the Arctic Ocean is
 385 driven by net terrestrial exchange. Near Iceland, ocean exchange contributes 10–20 % of the
 386 overall seasonal cycle amplitude but the ocean component is otherwise small (Fig. S2), following
 387 what has been documented about continental Arctic CO₂ mixing ratios (e.g. Graven et al., 2013).
 388 From Figure S2, we see that the region around Alert and Ellesmere Island is predicted to have a
 389 smaller CO₂ amplitude than anywhere else in the Arctic. The sparse tundra vegetation on these
 390 high Arctic islands, including around Alert, NU, contributes little to the seasonal cycle of CO₂
 391 uptake and release. This region is also where others have identified the polar dome airmass in
 392 spring (Bozem et al., 2019; Stohl, 2006), consistent with inhibited transport causing the small
 393 amplitudes at Alert. Thus, while these features of the atmospheric CO₂ seasonal cycle over the

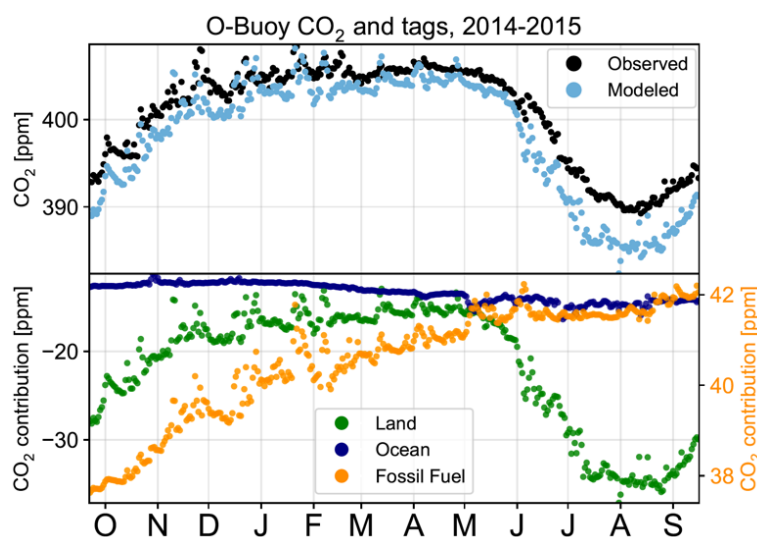


Figure 4. CO₂ mixing ratios in observations and model (top) and simulated contributions from key sources (bottom). All data are daily averages at the O-Buoys from October 2014 through September 2015. Read land and ocean contributions on the left axis and fossil fuel contribution on the right axis. Contributions to total CO₂ from biomass burning and atmospheric chemistry do not contribute to variability seen in the figures and are therefore not shown.

Arctic Ocean have not previously been reported, they can be explained through terrestrial CO₂ sources and transport, without requiring large CO₂ fluxes over or through sea ice. Fluxes over sea ice may contribute to other aspects of CO₂ variability over the Arctic Ocean, however, as will be discussed in Section 3.4.

Atmospheric CO₂ mixing ratios at the O-Buoys were obtained during times of varying sea ice cover (Fig. 2d, 5). There is a seasonal cycle of sea ice that corresponds to the seasonal cycle of CO₂, with minima occurring annually around September. The wintertime freeze is apparent with sea ice concentrations reaching 100 % at the majority of O-Buoys, with some variability evident. Most of the high-frequency variability of sea ice concentration occurs during the warmer months, presumably when sea ice is melting and winds shift sea ice at a higher frequency (Fig. 2d).

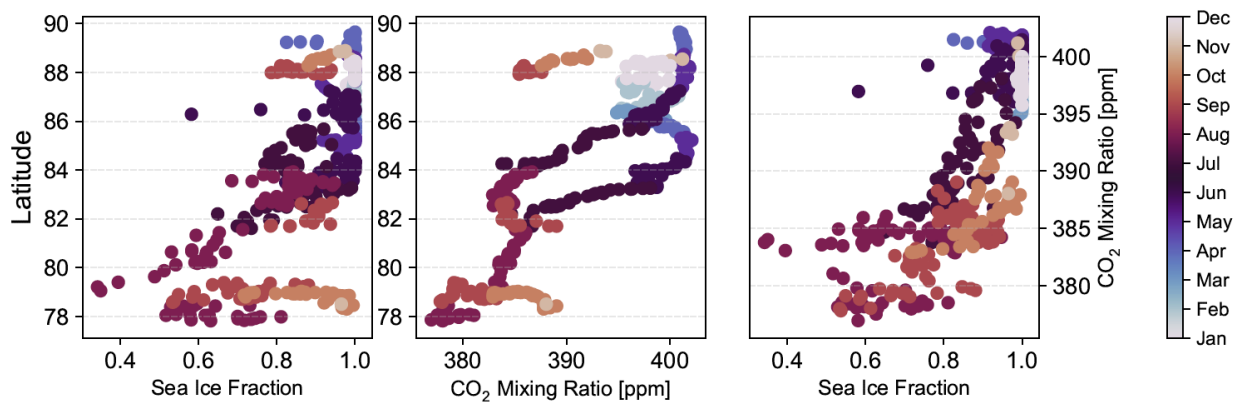


Figure 5. Relationships between CO₂ mixing ratio, sea ice concentration, and latitude for O-Buoys 5 (Beaufort Gyre), 4 and 6 (central Arctic through Fram Strait), which were deployed 2011–2012. Colors show the month of observation. All data are daily means.

During 2011–2012, the lowest CO₂ mixing ratios were measured in August and September, even at latitudes higher than 78 °N when sea ice concentration was 50–70 %, on average (Fig. 5). Mid-range CO₂ mixing ratios were usually recorded in late spring and fall (385–395 ppm) regardless of latitude, with the highest values in winter and early spring (> 400 ppm). The April–May O-Buoy observations were collected during mostly complete or complete sea ice cover, with varying snow cover (Webster et al., 2018). At the time of the August–September minima, sea ice concentration was 80 % or less, a direct result of the seasonal cycle of sea ice. During the 2011–2012 period, buoys measured in areas with sea ice concentration as low as 30 %. Once the sea ice broke up, however, early O-Buoys (1–4) stopped data collection when they became free floating and unable to remain upright.

3.2 CO₂ sub-monthly temporal variability

Close inspection of Figure 2 suggests that day-to-day CO₂ variations are larger in summer and fall than spring. Figure 6 highlights the magnitude of this sub-monthly temporal variability, averaged across years. At the O-Buoys and Utqiagvik, AK, day-to-day variability is

smallest (standard deviation < 1 ppm) in March–May and increases two-fold or more through summer into early winter (1–2 ppm). Sub-monthly variability is also greater at Utqiagvik, AK than at the O-Buoys over sea ice, particularly in the fall when it reaches about 2 ppm at Utqiagvik. Both locations have an initial peak variability in July, then hold steady or slightly decrease before reaching their annual maximum variability in fall. Over sea ice, the model predicts larger amplitudes of sub-monthly variability than was observed throughout the entire seasonal cycle, consistent with the model overestimation of the annual CO₂ amplitudes. The model also overpredicts the amplitudes of sub-monthly variability during most of the annual cycle at Utqiagvik, AK, except in the late summer and fall. At both locations, the largest model overestimation is during July.

Figure 4 shows that observed sub-monthly CO₂ variations at the O-Buoys are predicted by the model and nearly all attributable to variations in CO₂ from net terrestrial exchange, indicated by the net terrestrial biosphere flux tag (i.e., land). While CO₂ from fossil fuel also correlates with the sub-monthly variability in the model, fossil fuel contributes little to the overall variability in CO₂ because of its smaller magnitude of variation. The sign of correlation between net terrestrial exchange and fossil fuel CO₂ also changes with season. In winter, terrestrial exchange is a source of CO₂ to the atmosphere, so it is positively correlated with fossil fuel CO₂. In the summer, land becomes a sink for atmospheric CO₂ and the correlation with fossil fuel CO₂ turns negative. The fluxes of CO₂ from fossil fuels in the Arctic are small and uncorrelated with net terrestrial exchange, so the correlation of these CO₂ tags in the model is due to their joint transport into the Arctic from lower latitudes. This means that the sub-monthly

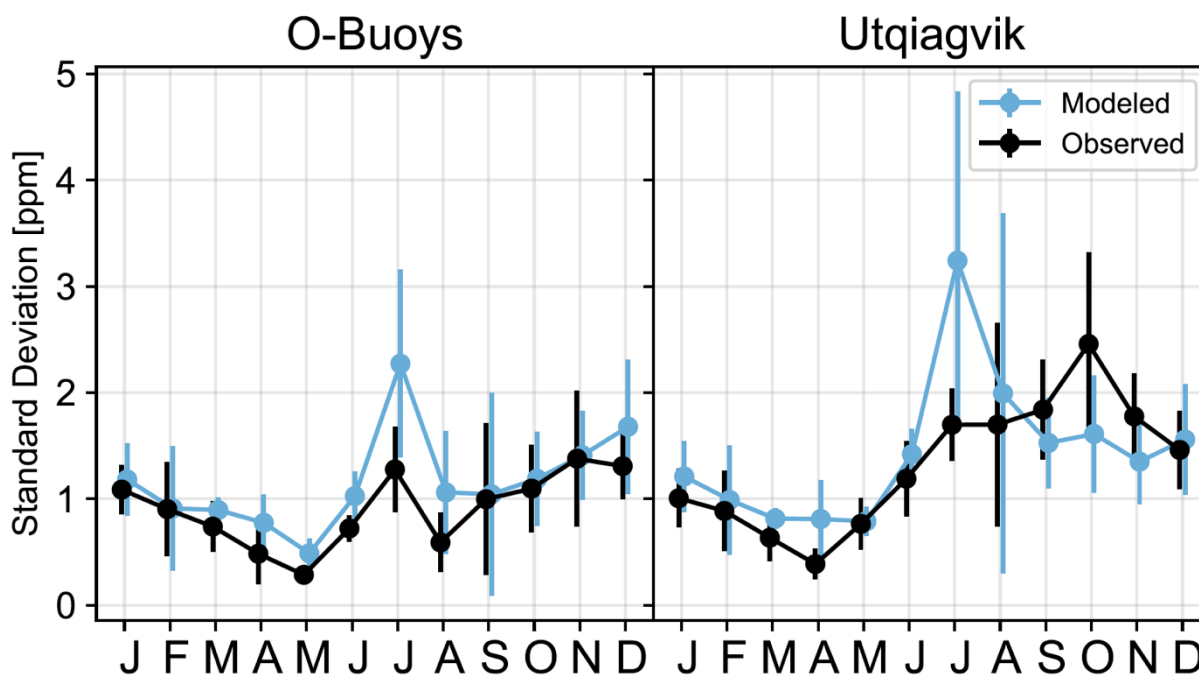


Figure 6. Variability of CO₂ mixing ratios within each month of the year. Points show standard deviations of CO₂ mixing ratio after removing the seasonal cycle, averaged monthly across all years (2009–2016). Vertical bars show interannual variability of the standard deviation.

CO₂ variability seen in observations and the model in Figure 4 is primarily due to long-range transport, rather than local sources and sinks. Transport has been found to dominate day-to-day variability of CO₂ mixing ratios at the surface in the midlatitudes (Parazoo et al., 2008) as well as within the total column of CO₂ across many latitudes (Jacobs et al, 2021; Keppel-Aleks et al., 2011, 2012). Results from Barnes et al. (2016) found that transport from the midlatitudes, rather than surface fluxes, dominates the seasonal cycle amplitudes at high latitudes. Our work shows that transport from lower latitudes explains most of the high-frequency variability observed at the O-Buoys, even though our observations are at the surface. Finally, the biomass burning and atmospheric chemistry seasonal patterns do not contribute to the sub-monthly variability in CO₂ mixing ratios (data not shown).

The ratio of observed:modeled standard deviations (Fig. 6, mean ratio of 0.78 at the O-Buoys) is similar to the ratio of observed:modeled seasonal amplitude value of 0.77 at the O-Buoys (i.e. the observed CO₂ seasonal amplitude is 77 % of the modeled CO₂ seasonal amplitude on average at the O-Buoys, Table 2), as discussed in Section 3.1. Since transport is the primary driver of the seasonal cycle amplitudes and high-frequency variability, this model underestimation is likely due to transport error within MERRA-2 reanalysis (Schuh et al., 2019). Schuh et al. (2019) found an excess of CO₂ near the surface at the northern high-latitudes likely due to errors insufficient vertical mixing in the boundary layer and lower troposphere.

We found no clear pattern between the high-frequency variability of sea ice concentrations and CO₂ mixing ratios. For the O-Buoys, we analyzed the Pearson correlation coefficients between both, each with the respective seasonal cycles removed, but found no compelling or consistent relationships, all of which are reported in Supplemental Table 5. Large correlation coefficients in winter (e.g., January where $p < 0.05$) are likely an artifact of the smoothing method, since the sea ice concentration is at or near 100 %.

3.3 CO₂ interannual variability

Figure 7 shows interannual variation of CO₂ mixing ratios for the annual maxima (April–May) and minima (August–September). The dominant feature in both seasons is the increase in CO₂ mixing ratios year after year, which is a global phenomenon. At coastal sites, CO₂ minimum mixing ratios grew slightly faster in August–September (2.4 ± 0.1 ppm yr⁻¹) than maximum mixing ratios in April–May (2.3 ± 0.0 ppm yr⁻¹; $p = 0.13$ for difference, two-sample z-test; Table S2). Over sea ice, CO₂ mixing ratios grew slower (2.1 ± 0.02 ppm yr⁻¹) than the coastal sites in both seasons. While the difference in growth rates between coastal sites and ice appears significant ($p < 0.001$), the diverging trends reported here for 2009–2016 may not be sustained over longer periods. Instead, the differing trends likely reflect both differences in the buoys' sampling locations in each year, as well as real differences in interannual CO₂ variability over sea ice versus coastal sites.

The interannual variability around the overall increasing trend is broadly similar at all of the coastal sites (Fig. 7), particularly in August–September at Alert, Utqiagvik, and Ny-Alesund. At all of these sites, CO₂ growth was largest (3–4 ppm yr⁻¹) in years 2009–2010, 2012–2013, and

479 2015–2016. The smallest CO₂ growth (0–1 ppm yr⁻¹) occurred in years 2010–2011 and 2013–
 480 2014. There is also coherent interannual variation in CO₂ growth among the coastal sites during
 481 April–May, but the deviations from the overall increasing trend are smaller, so we focus on
 482 interpreting the summer patterns below. Over the sea ice, the interannual CO₂ variability at the
 483 O-Buoys is different from the coastal sites. In August–September, CO₂ growth was largest in
 484 2011–2012 (5 ppm yr⁻¹) and smallest in 2015–2016, neither of which corresponds with features
 485 at coastal sites.

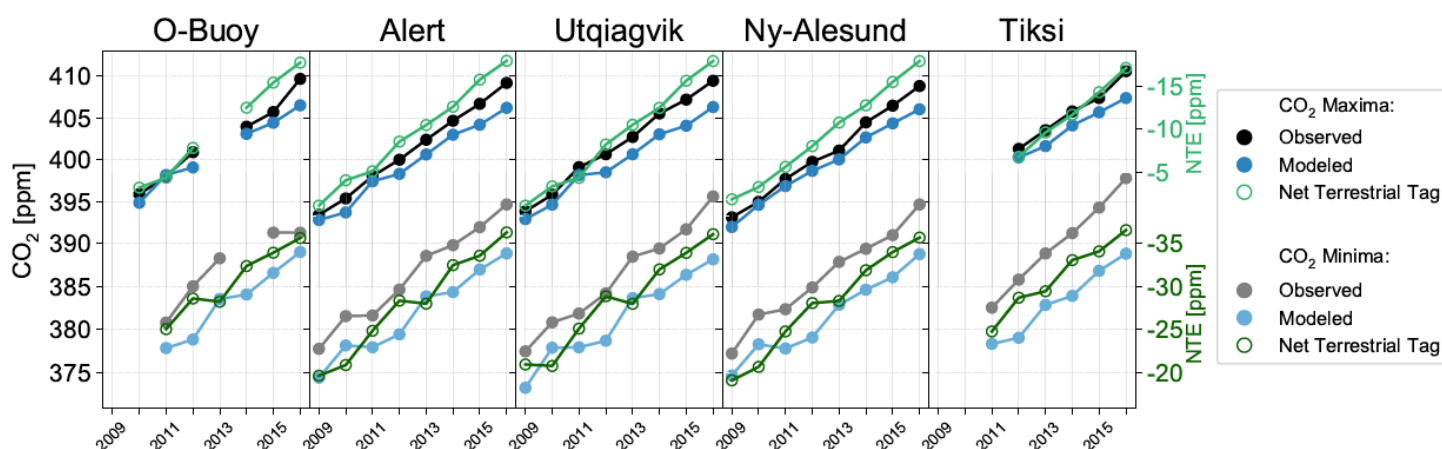


Figure 7. Trends and interannual variability of CO₂ at the O-Buoys and land stations during April–May (“CO₂ Maxima”) and August–September (“CO₂ Minima”). Results are shown for observations and model. Note that net terrestrial exchange (NTE) axis is inverted and negative NTE removes CO₂ from the atmosphere.

486 GEOS-Chem predictions are consistent with observations for years of largest and
 487 smallest CO₂ growth at the coastal sites, and the CO₂ source tracers identify the causes. As seen
 488 in Figure 7, CO₂ from net terrestrial flux can explain the sign and magnitude of interannual
 489 variability at the coastal sites. We examined all other CO₂ source tags, but found that they
 490 contributed relatively little to interannual variability (as discussed previously), so they are not
 491 shown. During years with large CO₂ growth (2009–2010, 2012–2013, and 2015–2016), the net
 492 terrestrial biosphere uptake from the atmosphere was slower than average; during the small CO₂
 493 growth years, the net uptake was larger than average. Past studies suggest the reasons for these
 494 interannual variations in net terrestrial flux. In summer 2009, the Arctic tundra was less green
 495 than normal (suggesting lower net primary productivity), due to a spike in atmospheric aerosols
 496 including volcanic dust, and cool summer temperatures (Walker et al., 2011). Less observed
 497 greening explains the large CO₂ growth from 2009–2010. In 2010 and 2011, the Arctic was
 498 greener than 2009, explaining the slow CO₂ growth from 2010–2011 (Walker et al., 2011;
 499 Epstein et al., 2013). Thus, the observed interannual variations in CO₂ minima at Arctic coastal
 500 sites are consistent with variations in the terrestrial biosphere that are already constrained by
 501 CarbonTracker inversion fluxes, as implemented in GEOS-Chem.

Over sea ice at the O-Buoys, GEOS-Chem predicts that interannual CO₂ variability in summer should be similar to the coastal sites, with the same years of highest and lowest growth, for the same reasons tied to net terrestrial flux. The observations, however, show different interannual variability from the coastal sites, as noted above. It appears, therefore, that there is an additional driver of interannual CO₂ variability over the Arctic Ocean, which is not represented in GEOS-Chem and has minimal influence on Arctic coastal sites. Air-sea or air-ice fluxes over the Arctic Ocean may be the missing process, since, like many atmospheric CO₂ models, GEOS-Chem currently neglects these fluxes over sea ice.

We speculate what might drive the missing surface flux over the Arctic Ocean based on known interannual variability in Arctic Ocean sea ice and seasonal weather. From 2011–2012, CO₂ growth was large over sea ice (5 ppm yr⁻¹), unlike coastal sites. O-Buoys in 2011 observed in the Beaufort Gyre (OB5) and Central Arctic (OB4), and in 2012 observed in the Fram Strait (OB4 and OB6) and Beaufort Gyre (OB8). Between these two summers, the Arctic Ocean saw a net loss of sea ice; the minimum area in 2011 was 4.33 million km², and in 2012 was 3.41 million km² (NSIDC). It has been noted that this ocean is acting as a net sink of CO₂ (Bates et al., 2011; MacGilchrist et al., 2014). However, as sea ice continues to decline (Perovich et al., 2020), it has also been pointed out that this air-sea exchange lacks uniformity (Bates et al., 2006; Nomura et al., 2018), and the Arctic Ocean may also act as a source of CO₂ to the atmosphere at times (Bates et al., 2011; Cai et al., 2010; MacDonald et al., 2010; Popova et al., 2014). Release of CO₂ from Arctic waters in years with low sea ice could contribute to the greater interannual increase of CO₂ over sea ice compared to land (Loose et al., 2011).

Between 2015–2016, the O-Buoys observed within the Beaufort Gyre (OB11, OB13, OB14) and East Siberian Sea (OB8, OB15), and showed little to no growth of CO₂ during the minima. The opposite occurred over land and within GEOS-Chem. Sea ice area declined at the O-Buoys (Fig. S3) and overall between these two years, with minimum area values at 4.63 million km² in 2015, and 4.14 million km² in 2016 (NSIDC). The lower value of local sea ice coverage may contribute to larger CO₂ uptake in ice-free waters near the O-Buoys, due to the regional variability of CO₂ sources and sinks. At the coastal stations, increased Arctic greening was observed in 2015 and 2016 (compared to 2014), though the North Slope of Alaska has been greening continuously throughout the long-term record (Richter-Menge et al., 2016). Despite this observed greening (and thus an increased plant uptake of CO₂), the observed interannual growth is large on land from 2014–2016. Possible explanations include CO₂ release from near-shore waters of the Arctic Ocean, where the marine microbial ecosystem is largely heterotrophic during this time of year (Carmack & Wassmann, 2006). Furthermore, newly ice-free waters exposed to enhanced wind-caused turbulence can experience enhanced upwelling (Mundy et al., 2009; Tremblay et al., 2011), that may episodically bring CO₂-rich waters into contact with the atmosphere, thus acting as a CO₂ source (Else et al., 2012a; Else et al., 2012b; Lansard et al., 2012; Mathis et al., 2012; Mucci et al., 2010).

3.4 Case studies of CO₂ spatial gradients

Looking at the overall time series of CO₂ mixing ratios (Fig. 2a and 2b), we chose to further examine two periods with notable differences between the coastal locations and O-Buoys: the annual cycle from 2011–2012, and winter to spring from 2014–2015. These periods had co-observing O-Buoys, which improved comparison for a case study. The following subsections examine these time periods in detail and explore possible causes of the CO₂ spatial gradients.

3.4.1 Annual cycle 2011–2012

Our first case study is 2011–2012 when three O-Buoys were sampling simultaneously. O-Buoys 4 and 6 deployed in the Central Arctic, then flowed through Fram Strait, while O-Buoy 5 deployed in the Beaufort Gyre (Fig. 1). O-Buoy 4 measured for almost an entire year, from fall 2011 through summer 2012. O-Buoy 5 sampled from summer 2011 through winter 2012, and O-Buoy 6 observed from late spring through summer 2012. During this time, the buoys ranged 420–1500 km from Alert, NU the closest coastal CO₂ measuring station on average.

The mean O-Buoy CO₂ mixing ratios were lower than nearby Alert, NU by 1.6 ± 1.5 ppm in winter (January–March) and higher by 0.9 ± 0.7 ppm in spring (April–May) (Fig. 2b). The model, however, predicts O-Buoy mixing ratios higher than Alert, NU in January–March (Fig. 2c). For March–May, the O-Buoys saw an increase of about 7 ppm, while Alert, NU only measured an increase of about 1–2 ppm. The observed patterns from March–May also go uncaptured by the model, which simulated an increase of about 3 ppm at the O-Buoys, and about 2 ppm at Alert, NU. The failure of the model to properly capture the large increase in CO₂ mixing ratio over sea ice reflects the difficulty to capture the possible processes occurring over land (transport) and sea ice (ocean flux processes).

Throughout the winter and into spring, a larger and more variable simulated TSCS was measured at Alert, NU than at the O-Buoys, suggesting mid-latitude free tropospheric entrainment (or relatively less vertical mixing) to the Arctic Ocean. This pattern reverses in the early summer, when the TSCS is greater over the O-Buoys than at Alert, NU. Both locations experience greater contact with sea ice than with land or open ocean for the majority of the shown time series (Fig. S4).

3.4.2 Winter and spring of 2014–2015

From the end of 2014 through spring 2015, O-Buoys 11 and 12 drifted in the Beaufort Gyre, less than 1000 kilometers from Utqiagvik, AK (Fig. 1). The O-Buoys routinely measured smaller CO₂ mixing ratios than at nearby Utqiagvik, AK from December 2014 through May 2015, averaging 1.2 ± 1.8 ppm lower (Fig. 2b). The model predicted CO₂ mixing ratios to be greater at the O-Buoys than at Utqiagvik, AK by about 0.5 ppm on average (Fig. 2c).

574 Though similar surface contact tracers were modeled at both locations, greater sea ice
 575 influence was modeled at the O-Buoys than at the coast, with greater land contact modeled at
 576 Utqiagvik, AK than at the O-Buoys (Fig. S6). The TSCS remains relatively constant over the
 577 Arctic Ocean throughout this period (Fig. 8). Over land, the TSCS decreased from winter to
 578 spring inland, but not at the coast. An isolating Arctic dome may be responsible for the winter
 579 stagnation over the sea ice (Stohl, 2006), and thus resulted in smaller CO₂ mixing ratios observed
 580 at the O-Buoys. In addition, the location of the atmospheric polar front separates colder Arctic
 581 and warmer polar continental air masses, which tends to correspond to the sea ice edge
 582 (Zakharov, 1997) and may have separated the air sampled by the O-Buoys from air over
 583 Utqiagvik, AK. Conversely, the winter-elevated CO₂ mixing ratios over coastal Alaska have
 584 been ascribed both to the transfer from the ocean via ocean-sea ice-atmosphere fluxes and/or to
 585 the atmospheric transport from mid-latitudes sources, similar to those for Arctic haze (Halter et

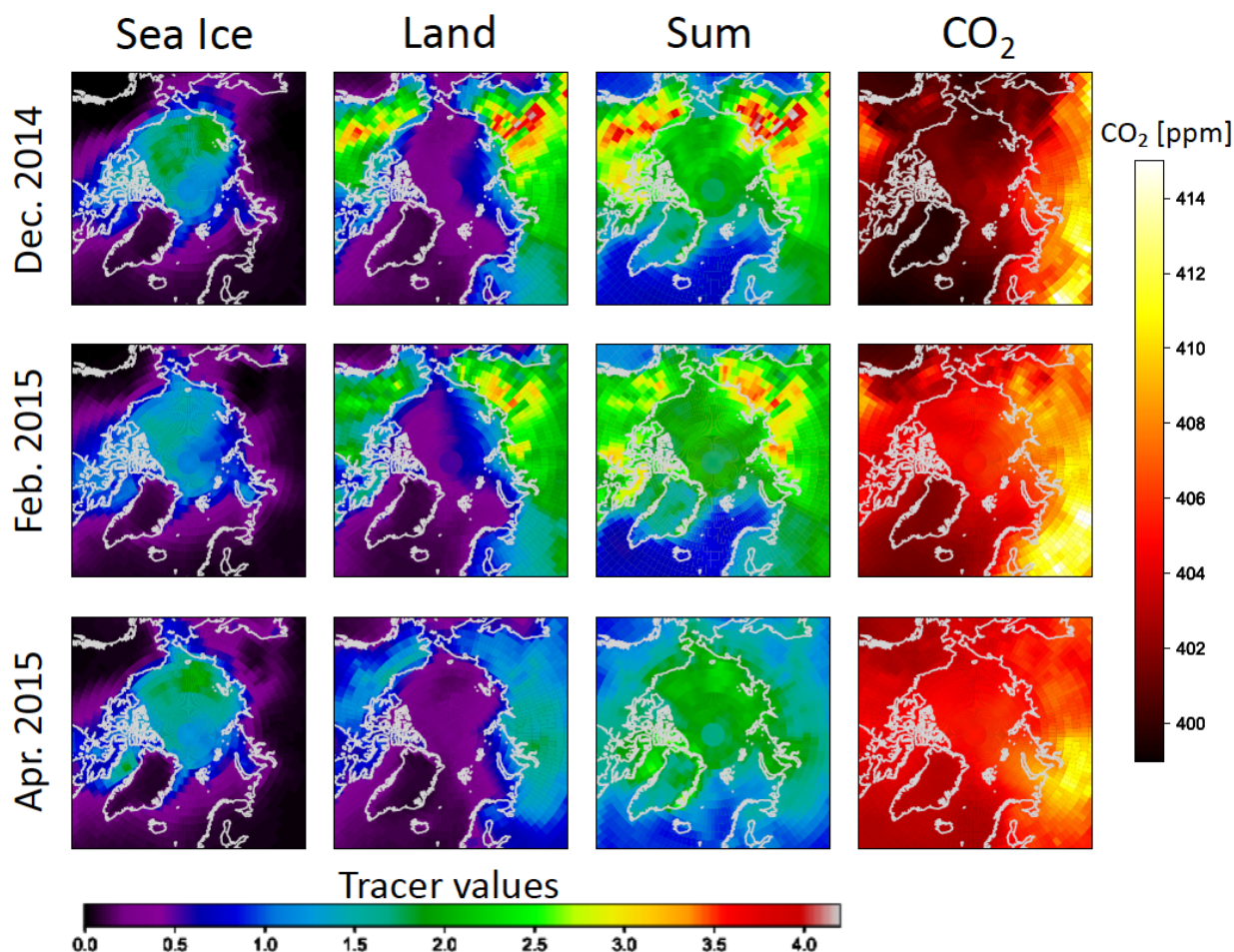


Figure 8. Simulated CO₂ mixing ratios and surface contact tracers during the winter to spring season 2014–2015. Tracer results are shown in columns 1 through 3, a polar view of each contact tracer with a 5-day lifetime (bottom color-bar indicates respective magnitude of contact with each surface type). The last column shows simulated CO₂ mixing ratios for the corresponding months (units in ppm).

al., 1985; Peterson et al., 1980), which may have contributed to the larger CO₂ mixing ratios observed at Utqiagvik, AK during this time period.

4 Conclusions

We obtained and analyzed measurements of atmospheric CO₂ mixing ratio from thirteen overlapping autonomous ice-tethered buoys in the ice-covered Arctic Ocean, part of the O-Buoy Network of Chemical Sensors (Knepp et al., 2010), as well as from coastal Arctic stations (Alert, NU; Utqiagvik, AK; Ny-Alesund, Svalbard; Tiksi, Russia) during the period 2009–2016. In our analysis, we evaluated seasonal, interannual, and sub-monthly variability evident within the observed values over sea ice and discussed the processes responsible for these observed patterns. The on-ice CO₂ mixing ratio observations were compared to nearby coastal station observations, to identify and understand differences between CO₂ over sea ice and over coasts. The surface CO₂ measurements were then compared to an updated version of the GEOS-Chem CO₂ model, to provide additional insight into how these CO₂ mixing ratios can be interpreted. Additionally, transport diagnostics were used to understand surface contact at our points and locations of interest. Observed CO₂ mixing ratios were also compared with remotely sensed sea ice concentrations.

Atmospheric CO₂ mixing ratios over Arctic sea ice showed multi-year trends in annual growth rate that are similar to those observed at nearby coastal sites. At these high latitude surface locations, our model tags showed that the terrestrial biosphere exchange dominates the annual seasonal CO₂ cycle, which follows expected behavior. However, the O-Buoy observations displayed smaller seasonal amplitudes than their nearby coastal counterparts on average, defying the conventional expectation that seasonal cycles only increase poleward. Similarly, CO₂ mixing ratios over sea ice were observed to be equal or smaller than at the coastal stations during most winters, contradicting the idea that CO₂ mixing ratios increase poleward during the winter months. While this conclusion considers latitude as the dependent variable, we can broaden our expectations of seasonal cycle amplitudes if we consider the magnitude and exchange of nearby terrestrial sources and sinks, which the Arctic Ocean lacks.

GEOS-Chem tended to overestimate the seasonal CO₂ cycle, particularly in the summer months, both at the coastal stations and over sea ice. From our analysis of CO₂ tags and high-frequency CO₂ variability, we found that vertical transport error may cause the magnitude of the seasonal cycle and sub-monthly CO₂ variability to be overestimated.

At coastal locations, interannual CO₂ growth was observed to be greater during the CO₂ minima (August–September) than during the maxima (April–May). Similar growth patterns were observed at Alert, NU, Utqiagvik, AK, and Ny-Alesund, Svalbard. The years with slower CO₂ growth were likely due to enhanced tundra greening, providing a pathway for net CO₂ drawdown into the terrestrial biosphere. On the contrary, when these three coastal stations observed quicker CO₂ growth, it was likely due to conditions promoting less greening in the Arctic terrestrial vegetation.

Interannual CO₂ growth was typically captured by GEOS-Chem, especially over the coastal stations. The model was unable to capture the distinct interannual variability observed over sea ice, particularly during the CO₂ minimum season. While the model provides insight that transport is the main driver of variability over sea ice, it is also plausible that a marine component of CO₂ gas exchange is impacting the interannual variability, which is not currently present within GEOS-Chem for sea ice. In our results, we showed examples where ocean uptake or release may have played a role in the interannual variability between CO₂ mixing ratios observed over sea ice and over the nearby coasts. Release of CO₂ from Arctic waters in years with low sea ice could contribute to the greater interannual increase of CO₂ over sea ice compared to land. While this provides evidence for interannual variability attributed to ocean exchange, no clear or compelling connection was found between high-frequency variability of CO₂ and sea ice concentrations.

The differences that exist between observed CO₂ mixing ratios at coastal stations and over sea ice provide insight into the physical mechanisms that influence its variability. Transport acts as the primary driver of gradients over sea ice and at the coastal stations on seasonal and synoptic timescales. This was well predicted by the model, which confirmed that seasonal variability at these latitudes is dominated by terrestrial biosphere exchange. While the model performed well overall, the interannual variability of CO₂ mixing ratios over sea ice was not adequately reproduced. This poor performance suggests that ocean processes, which are currently neglected in atmospheric models like GEOS-Chem, may play a role in moderating the interannual variability of CO₂ over sea ice. As a whole, this work demonstrates the value of continuous atmospheric CO₂ observations over sea ice as the Arctic warms and high-latitude carbon reservoirs changes.

Acknowledgments

We are deeply indebted to the rest of the O-Buoy Team through the years for their invaluable input and dedication with designing, building, deploying (*), communicating and controlling all O-Buoys: D. Carlson*, P. Peterson* and S. Walsh* (UAF); B. Tupper (Bigelow); B. Elder, T. Tantilillo (CRREL); S. Netcheva* (Environment Canada); C. Wahl (MBARI); M. Carlsen, J. Davison, R.M. Everlee, T. Knepp*, R. Oglesbee, R. Santini, P. J. Wyss and J. Zimmermann (Purdue); and last but not least T. Valentic and R. Stehle (SRI). J. Sevadjan, D. Northcott and D. Sancho-Gallegos (MBARI) contributed to CO₂ data analysis. O-Buoy deployments were achieved through a long-lasting collaboration with the Beaufort Gyre Exploration Project Team, especially R. Krishfield and J. Toole (WHOI) as well as W. Williams, S. Zimmermann and J. Eert (DFO-MPO, Environment Canada) on Canadian Coast Guard icebreakers, especially CCG St. Laurent; with I. Polyakov (UAF) and the NABOS Team on Russian icebreakers; with J. Verhoef and D. Mosher (2011 US-Canadian Extended Continental Shelf Mapping Program) on the CCG St. Laurent and S. Gerland (NPI) on the R/V Lance; and finally with J. Morison, A. Heiberg and D. Stewart (PSC APL UW) at the Barneo NPEO. Funding was provided by U.S. NSF OPP AON for the original O-Buoy measurements to PAM,

FPC, DKP, PBS, and WRS as well as by Environment Canada to JWB. Funding for data analyses and modeling was provided by U.S. NSF OPP ANS to WRS, FPC, CDH, PAM, and DKP. Funding for graduate studies of KAG was provided by the NASA Earth and Space Science Fellowship.

PAM, JWB, FPC, DKP, PBS and WRS conceived, funded and implemented the original O-Buoy Chemical Network that provided CO₂ data. GF, CDR, CRW, PKP, and JWH built and/or deployed the CO₂ sensors and/or O-Buoys. DKP led the sea ice data analysis. PPT provided access to land station CO₂ data. KAG and CDH provided all modeling runs. KAG, DH, JWH and PAM led data analysis and manuscript preparation. All co-authors read and commented on the manuscript.

This work was supported by the NSF Office of Polar Programs (grants 1602946, 1602883, 1602883, 1602716, and 1603172) and by a NASA Earth and Space Science Fellowship to KAG (grant 80NSSC17K0361)

The authors declare not having any competing interests.

Open Research

All O-Buoy data are available at the National Science Foundation Arctic Data Center (<https://arcticdata.io/>). All land station data are available at National Oceanographic and Atmosphere Administration Earth System Research Laboratory Global Greenhouse Gas Reference Network (<https://www.esrl.noaa.gov/gmd/ccgg/>). All sea ice concentration data are available at the National Snow and Ice Data Center (<https://nsidc.org/data/nsidc-0051>). CarbonTracker CT2019 results provided by NOAA ESRL, Boulder, Colorado, USA from the website at <http://carbontracker.noaa.gov>. GEOS-Chem source code can be obtained at www.geos-chem.org and model output used in this manuscript are available from Zenodo (DOI provided after acceptance).

References

- Bacastow, R. B., Keeling, C. D., & Whorf, T. P. (1985). Seasonal amplitude increase in atmospheric CO₂ concentration at Mauna Loa, Hawaii, 1959-1982. *Journal of Geophysical Research*, 90(D6), 10539–10540. <https://doi.org/10.1029/JD090iD06p10529>
- Barnes, E. A., Parazoo, N., Orbe, C., & Denning, A. S. (2016). Isentropic transport and the seasonal cycle amplitude of CO₂. *Journal of Geophysical Research: Atmospheres*, 121(13), 8106–8124. <https://doi.org/10.1002/2016JD025109>
- Bates, N. R., Moran, S. B., Hansell, D. A., & Mathis, J. T. (2006). An increasing CO₂ sink in the Arctic Ocean due to sea-ice loss. *Geophysical Research Letters*, 33(23). <https://doi.org/10.1029/2006GL027028>
- Bates, N. R., Cai, W.-J., & Mathis, J. T. (2011). The Ocean Carbon Cycle in the Western Arctic Ocean: Distributions and Air-Sea Fluxes of Carbon Dioxide. *Oceanography*, 24(3), 186–201. <https://doi.org/10.5670/oceanog.2011.71>
- Bozem, H., Hoor, P., Kunkel, D., Köllner, F., Schneider, J., Herber, A., et al. (2019). Characterization of transport regimes and the polar dome during Arctic spring and summer using in situ aircraft measurements. *Atmospheric Chemistry and Physics*, 19(23), 15049–15071. <https://doi.org/10.5194/acp-19-15049-2019>
- Bukosa, B., Fisher, J., Deutscher, N., and Jones, D. (2021). An improved carbon greenhouse gas simulation in GEOS-Chem version 12.1.1. *Geoscientific Model Development Discussion*. [preprint], <https://doi.org/10.5194/gmd-2021-173>, in review.
- Burd, J. A., Peterson, P. K., Nghiem, S. V., Perovich, D. K., & Simpson, W. R. (2017). Snowmelt onset hinders bromine monoxide heterogeneous recycling in the Arctic. *Journal of Geophysical Research: Atmospheres*, 122, 8297–8309. <https://doi.org/10.1002/2017JD026906>
- Cai, W.-J., Chen, L., Chen, B., Gao, Z., Lee, S. H., Chen, J., et al. (2010). Decrease in the CO₂ Uptake Capacity in an Ice-Free Arctic Ocean Basin. *Science*, 329(5991), 556–559. <https://doi.org/10.1126/science.1189338>
- Cai, W.-J., Bates, N. R., Guo, L., Anderson, L. G., Mathis, J. T., Wanninkhof, R., et al. (2014). Carbon Fluxes Across Boundaries in the Pacific Arctic Region in a Changing Environment. In J. M. Grebmeier & W. Maslowski (Eds.), *The Pacific Arctic Region: Ecosystem Status and Trends in a Rapidly Changing Environment* (pp. 199–222). Dordrecht: Springer Netherlands. https://doi.org/10.1007/978-94-017-8863-2_8
- Carmack, E., & Wassmann, P. (2006). Food webs and physical-biological coupling on pan-Arctic shelves: Unifying concepts and comprehensive perspectives. *Progress in Oceanography*, 71(2–4), 446–477. <https://doi.org/10.1016/j.pocean.2006.10.004>
- Ciais, P., Sabine, C., Bala, G., Bopp, L., Brovkin, V., Canadell, J., et al. (2013). *Carbon and Other Biogeochemical Cycles*. In Stocker, T. F., et al. (Eds.), *Climate Change 2013: The Physical Science Basis. Contribution of Working Group I to the Fifth Assessment Report of the Intergovernmental Panel on Climate Change*. Cambridge University Press,

- Cambridge, United Kingdom and New York, NY, USA.
<https://doi.org/10.1017/CBO9781107415324>
- Comiso, J. C., Parkinson, C. L., Gersten, R., & Stock, L. (2008). Accelerated decline in the Arctic sea ice cover. *Geophysical Research Letters*, 35(1), 1–6.
<https://doi.org/10.1029/2007GL031972>
- Dlugokencky, E. J., Lang, P. M., Mund, J. W., Crotwell, A. M., Crotwell, M. J., & Thoning, K. W. (2016). Atmospheric carbon dioxide dry air mole fractions from the NOAA ESRL Carbon Cycle Cooperative Global Air sampling network, 1968–2015, Version: 2016-08-30, Retrieved from ftp://aftp.cmdl.noaa.gov/data/trace_gases/co2/flask/surface/.
- Elmendorf, S. C., Henry, G. H. R., Hollister, R. D., Björk, R. G., Boulanger-Lapointe, N., Cooper, E. J., et al. (2012). Plot-scale evidence of tundra vegetation change and links to recent summer warming. *Nature Climate Change*, 2(6), 453–457.
<https://doi.org/10.1038/nclimate1465>
- Else, B. G. T., Papakyriakou, T. N., Galley, R. J., Drennan, W. M., Miller, L. A., & Thomas, H. (2011). Wintertime CO₂ fluxes in an Arctic polynya using eddy covariance: Evidence for enhanced air-sea gas transfer during ice formation. *Journal of Geophysical Research: Oceans*, 116(C9). <https://doi.org/10.1029/2010JC006760>
- Else, B. G. T., Papakyriakou, T. N., Galley, R. J., Mucci, A., Gosselin, M., Miller, L. A., et al. (2012). Annual cycles of *p*CO_{2sw} in the southeastern Beaufort Sea: New understandings of air-sea CO₂ exchange in arctic polynya regions. *Journal of Geophysical Research: Oceans*, 117(C9). <https://doi.org/10.1029/2011JC007346>
- Else, B. G. T., Galley, R. J., Papakyriakou, T. N., Miller, L. A., Mucci, A., & Barber, D. (2012). Sea surface *p*CO₂ cycles and CO₂ fluxes at landfast sea ice edges in Amundsen Gulf, Canada. *Journal of Geophysical Research: Oceans*, 117(C9).
<https://doi.org/10.1029/2012JC007901>
- Else, B. G. T., Galley, R. J., Lansard, B., Barber, D. G., Brown, K., Miller, L. A., et al. (2013). Further observations of a decreasing atmospheric CO₂ uptake capacity in the Canada Basin (Arctic Ocean) due to sea ice loss. *Geophysical Research Letters*, 40(6), 1132–1137. <https://doi.org/10.1002/grl.50268>
- Epstein, H. E., Walker, D. A., Bhatt, U. S., Bieniek, P., Comiso, J., Pinzon, J., et al. (2013). Vegetation [in Arctic Report Card 2013], <https://www.arctic.noaa.gov/Report-Card>.
- Fisher, J. A., D. J. Jacob, M. T. Purdy, M. Kopacz, P. Le Sager, C. Carouge, et al. (2010). Source attribution and interannual variability of Arctic pollution in spring constrained by aircraft (ARCTAS, ARCPAC) and satellite (AIRS) observations of carbon monoxide. *Atmospheric Chemistry and Physics*, 10(3), 977–996. <https://doi.org/10.5194/acp-10-977-2010>
- Forkel, M., Carvalhais, N., Rödenbeck, C., Keeling, R., Heimann, M., Thonicke, K., et al. (2016). Enhanced seasonal CO₂ exchange caused by amplified plant productivity in northern ecosystems. *Science*, 351(6274), 696–699.
<https://doi.org/10.1126/science.aac4971>

- 766 Friedlingstein, P., Jones, M. W., O'Sullivan, M., Andrew, R. M., Hauck, J., Peters, G. P., et al.
767 (2019). Global Carbon Budget 2019. *Earth Syst. Sci. Data*, 11(4), 1783–1838.
768 <https://doi.org/10.5194/essd-11-1783-2019>
- 769 Geilfus, N.-X., Carnat, G., Papakyriakou, T., Tison, J.-L., Else, B., Thomas, H., et al. (2012).
770 Dynamics of $p\text{CO}_2$ and related air-ice CO_2 fluxes in the Arctic coastal zone (Amundsen
771 Gulf, Beaufort Sea). *Journal of Geophysical Research: Oceans*, 117(C9), C00G10.
772 <https://doi.org/10.1029/2011JC007118>
- 773 Geilfus, N.-X., Galley, R. J., Crabeck, O., Papakyriakou, T., Landy, J., Tison, J. L., & Rysgaard,
774 S. (2015). Inorganic carbon dynamics of melt-pond-covered first-year sea ice in the
775 Canadian Arctic. *Biogeosciences*, 12(6), 2047–2061. [https://doi.org/10.5194/bg-12-2047-](https://doi.org/10.5194/bg-12-2047-2015)
776 2015
- 777 Gelaro, R., McCarty, W., Suárez, M. J., Todling, R., Molod, A., Takacs, L., et al. (2017). The
778 modern-era retrospective analysis for research and applications, version 2 (MERRA-2).
779 *Journal of Climate*, 30(14), 5419–5454. <https://doi.org/10.1175/JCLI-D-16-0758.1>
- 780 Goetz, S. J., Bunn, A. G., Fiske, G. J., & Houghton, R. A. (2005). Satellite-observed
781 photosynthetic trends across boreal North America associated with climate and fire
782 disturbance. *Proceedings of the National Academy of Sciences*, 102, 13521–13525.
783 <https://www.doi.org/10.1073/pnas.0506179102>
- 784 Graven, H. D., Keeling, R. F., Piper, S. C., Patra, P. K., Stephens, B. B., Wofsy, S. C., et al.
785 (2013). Enhanced Seasonal Exchange of CO_2 by Northern Ecosystems Since 1960.
786 *Science*, 341(6150), 1085–1090. <https://www.doi.org/10.1126/science.1239207>
- 787 Groendahl, L., Friborg, T., & Soegaard, H. (2007). Temperature and snow-melt controls on
788 interannual variability in carbon exchange in the high Arctic. *Theoretical & Applied*
789 *Climatology*, 88(1–2), 111–125. <https://www.doi.org/10.1007/s00704-005-0228-y>
- 790 Halfacre, J. W., Knepp, T. N., Shepson, P. B., Thompson, C. R., Pratt, K. A., Li, B., et al. (2014).
791 Temporal and spatial characteristics of ozone depletion events from measurements in the
792 Arctic. *Atmospheric Chemistry and Physics*, 14, 4875–4894. [https://doi.org/10.5194/acp-](https://doi.org/10.5194/acp-14-4875-2014)
793 14-4875-2014
- 794 Halter, B. C., Harris, J. M., & Rahn, K. A. (1985). A study of winter variability in carbon dioxide
795 and Arctic haze aerosols at Barrow, Alaska. *Atmospheric Environment*, 19(12), 2033–
796 2037. [https://doi.org/10.1016/0004-6981\(85\)90111-8](https://doi.org/10.1016/0004-6981(85)90111-8)
- 797 Hoesly, R. M., Smith, S. J., Feng, L., Klimont, Z., Janssens-Maenhout, G., Pitkanen, T., et al.
798 (2018). Historical (1750–2014) anthropogenic emissions of reactive gases and aerosols
799 from the Community Emissions Data System (CEDS). *Geoscientific Model Development*,
800 11(1), 369–408. <https://doi.org/10.5194/gmd-11-369-2018>
- 801 Jacobs, N., Simpson, W. R., Graham, K. A., Holmes, C., Hase, F., Blumenstock, T., et al. (2021).
802 Spatial distributions of XCO_2 seasonal cycle amplitude and phase over northern high-
803 latitude regions. *Atmospheric Chemistry and Physics*, 21, 16661–16687.
804 <https://doi.org/10.5194/acp-21-16661-2021>

- Jacobson, A. R., Schuldt, K. N., Miller, J. B., Oda, T., Tans, P., Andrews, A., et al. (2020). CarbonTracker CT2019. NOAA Earth System Research Laboratory, Global Monitoring Division. <https://doi.org/10.25925/39M3-6069>
- Jutterström, S., & Anderson, L. G. (2010). Uptake of CO₂ by the Arctic Ocean in a changing climate. *Marine Chemistry*, 122(1–4), 96–104. <https://doi.org/10.1016/j.marchem.2010.07.002>
- Kasischke, E. S., Verbyla, D. L., Rupp, T. S., McGuire, A. D., Murphy, K. A., Jandt, R., et al. (2010). Alaska's changing fire regime - implications for the vulnerability of its boreal forests. *Canadian Journal of Forest Research*, 40(7), 1313–1324. <https://doi.org/10.1139/X10-098>
- Keeling, C. D., Chin, J. F. S., & Whorf, T. P. (1996). Increased activity of northern vegetation inferred from atmospheric CO₂ measurements. *Nature*, 382(6587), 146–148. <https://www.doi.org/10.1038/382146a0>
- Keppel-Aleks, G., Wennberg, P. O., & Schneider, T. (2011). Sources of variations in total column carbon dioxide. *Atmospheric Chemistry and Physics*, 11(8), 3581–3593. <https://doi.org/10.5194/acp-11-3581-2011>
- Keppel-Aleks, G., Wennberg, P. O., Washenfelder, R. A., Wunch, D., Schneider, T., Toon, G. C., et al. (2012). The imprint of surface fluxes and transport on variations in total column carbon dioxide. *Biogeosciences*, 9(3), 875–891. <https://doi.org/10.5194/bg-9-875-2012>
- Knepp, T. N., Bottenheim, J., Carlsen, M., Carlson, D., Donohoue, D., Friederich, G., et al. (2010). Development of an autonomous sea ice tethered buoy for the study of ocean-atmosphere-sea ice-snow pack interactions: The O-buoy. *Atmospheric Measurement Techniques*, 3(1), 249–261. <https://doi.org/10.5194/amt-3-249-2010>
- Lansard, B., Mucci, A., Miller, L. A., Macdonald, R. W., & Gratton, Y. (2012). Seasonal variability of water mass distribution in the southeastern Beaufort Sea determined by total alkalinity and δ¹⁸O. *Journal of Geophysical Research: Oceans*, 117(C3). <https://doi.org/10.1029/2011JC007299>
- Loose, B., Miller, L. A., Elliott, S., & Papakyriakou, T. (2011). Sea Ice Biogeochemistry and Material Transport Across the Frozen Interface. *Oceanography*, 24(3), 202–218. <https://doi.org/10.5670/oceanog.2011.72>
- Macdonald, R. W., Anderson, L. G., Christensen, J. P., Miller, L. A., Semiletov, I. P., & Stein, R. (2010). The Arctic Ocean: budgets and fluxes. In Liu, K.-K., Atkinson, L., Quinones R., & Talaue-McManus, L. (Eds) Carbon and nutrient fluxes in continental margins: a global synthesis, Global Change – The IGBP series (pp 290–303). Springer-Verlag Berlin Heidelberg.
- MacGilchrist, G. A., Naveira Garabato, A. C., Tsubouchi, T., Bacon, S., Torres-Valdés, S., & Azetsu-Scott, K. (2014). The Arctic Ocean carbon sink. *Deep-Sea Research Part I: Oceanographic Research Papers*, 86, 39–55. <https://doi.org/10.1016/j.dsr.2014.01.002>

- 843 Magnani, F., Mencuccini, M., Borghetti, M., Berbigier, P., Berninger, F., Delzon, S., et al.
844 (2007). The human footprint in the carbon cycle of temperate and boreal forests. *Nature*,
845 447(7146), 849–851. <https://doi.org/10.1038/nature05847>
- 846 Mathis, J. T., Pickart, R. S., Byrne, R. H., McNeil, C. L., Moore, G. W. K., Juranek, L. W., et al.
847 (2012). Storm-induced upwelling of high $p\text{CO}_2$ waters onto the continental shelf of the
848 western Arctic Ocean and implications for carbonate mineral saturation states.
849 *Geophysical Research Letters*, 39(7). <https://doi.org/10.1029/2012GL051574>
- 850 McGuire, A. D., Anderson, L. G., Christensen, T. R., Scott, D., Laodong, G., Hayes, D. J., et al.
851 (2009). Sensitivity of the carbon cycle in the Arctic to climate change. *Ecological*
852 *Monographs*, 79(4), 523–555. <https://doi.org/10.1890/08-2025.1>
- 853 McGuire, A. D., Macdonald, R. W., Schuur, E. A. G., Harden, J. W., Kuhry, P., Hayes, D. J., et
854 al. (2010). The carbon budget of the northern cryosphere region. *Current Opinion in*
855 *Environmental Sustainability*, 2(4), 231–236.
856 <https://doi.org/10.1016/j.cosust.2010.05.003>
- 857 McGuire, A. D., Anderson, L. G., Christensen, T. R., Dallimore, S., Guo, L., Hayes, D. J., et al.
858 (2014). Sensitivity of the Carbon Cycle in the Arctic to Climate Change of the carbon
859 cycle in the Arctic to climate change Sensitivity. *Ecological Monographs*, 79(4), 523–
860 555. <https://www.doi.org/10.1890/08-2025.1>
- 861 Meier, W. N., Stroeve, J., Barrett, A., & Fetterer, F. (2012). A simple approach to providing a
862 more consistent Arctic sea ice extent time series from the 1950s to present. *Cryosphere*,
863 6(6), 1359–1368. <https://doi.org/10.5194/tc-6-1359-2012>
- 864 Miller, L. A., Papakyriakou, T. N., Collins, R. E., Deming, J. W., Ehn, J. K., MacDonald, R. W.,
865 et al. (2011). Carbon dynamics in sea ice: A winter flux time series. *Journal of*
866 *Geophysical Research: Oceans*, 116(C2), C02028.
867 <https://doi.org/10.1029/2009JC006058>
- 868 Mucci, A., Lansard, B., Miller, L. A., & Papakyriakou, T. N. (2010). CO₂ fluxes across the air-
869 sea interface in the southeastern Beaufort Sea: Ice-free period. *Journal of Geophysical*
870 *Research: Oceans*, 115(C4). <https://doi.org/10.1029/2009JC005330>
- 871 Mundy, C. J., Gosselin, M., Ehn, J., Gratton, Y., Rossnagel, A., Barber, D. G., et al. (2009).
872 Contribution of under-ice primary production to an ice-edge upwelling phytoplankton
873 bloom in the Canadian Beaufort Sea. *Geophysical Research Letters*, 36(17).
874 <https://doi.org/10.1029/2009GL038837>
- 875 Myneni, R. B., Keeling, C. D., Tucker, C. J., Asrar, G., & Nemani, R. R. (1997). Increased plant
876 growth in the northern high latitudes from 1981 to 1991. *Nature*, 386, 698–702.
877 <https://www.doi.org/10.1038/386698a0>
- 878 Nassar, R., Jones, D. B. A., Suntharalingam, P., Chen, J. M., Andres, R. J., Wecht, K. J., et al.
879 (2010). Modeling global atmospheric CO₂ with improved emission inventories and CO₂
880 production from the oxidation of other carbon species. *Geoscientific Model Development*,
881 3(2), 689–716. <https://doi.org/10.5194/gmd-3-689-2010>

- 882 Nomura, D., Granskog, M. A., Assmy, P., Simizu, D., & Hashida, G. (2013). Arctic and
883 Antarctic sea ice acts as a sink for atmospheric CO₂ during periods of snowmelt and
884 surface flooding. *Journal of Geophysical Research: Oceans*, 118(12), 6511–6524.
885 <https://doi.org/10.1002/2013JC009048>
- 886 Nomura, D., Granskog, M. A., Fransson, A., Chierici, M., Silyakova, A., & Ohshima, K. I.
887 (2018). CO₂ flux over young and snow-covered Arctic pack ice in winter and spring.
888 *Biogeosciences*, 15, 3331–3343. <https://doi.org/10.5194/bg-15-3331-2018>
- 889 Oda, T., & Maksyutov, S. (2011). A very high-resolution (1 km × 1 km) global fossil fuel CO₂
890 emission inventory derived using a point source database and satellite observations of
891 nighttime lights. *Atmospheric Chemistry and Physics*, 11(2), 543–556.
892 <https://doi.org/10.5194/acp-11-543-2011>
- 893 Osborne, E., Richter-Menge, J., & Jeffries, M. (2018). Arctic Report Card 2018.
894 <https://www.arctic.noaa.gov/Report-Card>
- 895 Pan, Y., Birdsey, R. A., Fang, J., Houghton, R., Kauppi, P. E., Kerz, W. A., et al. (2011). A
896 Large and Persistent Carbon Sink in the World's Forests. *Science*, 333(6045), 988–993.
897 <https://www.doi.org/10.1126/science.1201609>
- 898 Parazoo, N. C., Denning, A. S., Kawa, S. R., Corbin, K. D., Lokupitiya, R. S., & Baker, I. T.
899 (2008). Mechanisms for synoptic variations of atmospheric CO₂ in North America, South
900 America and Europe. *Atmospheric Chemistry and Physics*, 8(23), 7239–7254.
901 <https://doi.org/10.5194/acp-8-7239-2008>
- 902 Perovich, D., Meier, W., Tschudi, M., Hendricks, S., Petty, A. A., Divine, D., et al. (2020). Sea
903 Ice [in Arctic Report Card 2020]. <https://doi.org/10.25923/n170-9h57>
- 904 Peterson, J. T., Hanson, K. J., Bodhaine, B. A., & Oltmans, S. J. (1980). Dependence of CO₂,
905 Aerosol, and Ozone Concentrations on Wind Direction at Barrow, Alaska During Winter.
906 *Geophysical Research Letters*, 7(5), 349–352. <https://doi.org/10.1029/GL007i005p00349>
- 907 Peterson, P. K., Simpson, W. R., & Nghiem, S. V. (2016). Variability of bromine monoxide at
908 Barrow, Alaska, over four halogen activation (March–May) seasons and at two on-ice
909 locations. *Journal of Geophysical Research: Atmospheres*, 121, 1381–1396.
910 <https://doi.org/10.1002/2015JD024094>
- 911 Popova, E. E., Yool, A., Aksenov, Y., Coward, A. C., & Anderson, T. R. (2014). Regional
912 variability of acidification in the Arctic: a sea of contrasts. *Biogeosciences*, 11(2), 293–
913 308. <https://doi.org/10.5194/bg-11-293-2014>
- 914 Prather, M. J., Zhu, X., Tang, Q., Hsu, J., & Neu, J. L. (2011). An atmospheric chemist in search
915 of the tropopause. *Journal of Geophysical Research: Atmospheres*, 116, D04306.
916 <https://doi.org/10.1029/2010JD014939>
- 917 Prytherch, J., Brooks, I. M., Crill, P. M., Thornton, B. F., Salisbury, D. J., Tjernström, M., et al.
918 (2017). Direct determination of the air-sea CO₂ gas transfer velocity in Arctic sea ice
919 regions. *Geophysical Research Letters*, 44(8), 3770–3778.
920 <https://doi.org/10.1002/2017GL073593>

- 921 Ramanathan, V., Lian, M. S., & Cess, R. D. (1979). Increased Atmospheric CO₂: Zonal and
922 Seasonal Estimates of the Effect on the Radiation Energy Balance and Surface
923 Temperature. *Journal of Geophysical Research*, 84(C8), 4949–4958.
924 <https://doi.org/10.1029/JC084iC08p04949>
- 925 Randerson, T., Thompson, V., Conway, J., Fung, I. Y., & Field, C. B. (1997). The contribution
926 of terrestrial sources and sinks to trends in the seasonal cycle of atmospheric carbon
927 dioxide. *Global Biogeochemical Cycles*, 11(4), 535–560.
928 <https://doi.org/10.1029/97GB02268>
- 929 Reichstein, M., Papale, D., Valentini, R., Aubinet, M., Bernhofer, C., Knohl, A., et al. (2007).
930 Determinants of terrestrial ecosystem carbon balance inferred from European eddy
931 covariance flux sites. *Geophysical Research Letters*, 34(1), L01402.
932 <https://doi.org/10.1029/2006GL027880>
- 933 Rennermalm, A. K., Henrik Soegaard, & Claus Nordstroem. (2005). Interannual Variability in
934 Carbon Dioxide Exchange from a High Arctic Fen Estimated by Measurements and
935 Modeling. *Arctic, Antarctic, and Alpine Research*, 37(4), 545–556.
936 [https://doi.org/10.1657/1523-0430\(2005\)037\[0545:IVICDE\]2.0.CO;2](https://doi.org/10.1657/1523-0430(2005)037[0545:IVICDE]2.0.CO;2)
- 937 Richter-Menge, J., Overland, J. E., & Mathis, J. T. (2016). Arctic Report Card 2016.
938 <http://www.arctic.noaa.gov/Report-Card>
- 939 Schuh, A. E., Jacobson, A. R., Basu, S., Weir, B., Baker, D., Bowman, K., et al.
940 (2019). Quantifying the impact of atmospheric transport uncertainty on CO₂ surface flux
941 estimates. *Global Biogeochemical Cycles*, 33, 484–500.
942 <https://doi.org/10.1029/2018GB006086>
- 943 Semiletov, I. P., Makshtas, A., Akasofu, S.-I., & L Andreas, E. (2004). Atmospheric CO₂
944 balance: The role of Arctic sea ice. *Geophysical Research Letters*, 31(5), n/a-n/a.
945 <https://doi.org/10.1029/2003gl017996>
- 946 Semiletov, I. P., Pipko, I. I., Repina, I., & Shakhova, N. E. (2007). Carbonate chemistry
947 dynamics and carbon dioxide fluxes across the atmosphere-ice-water interfaces in the
948 Arctic Ocean: Pacific sector of the Arctic. *Journal of Marine Systems*, 66(1–4), 204–226.
949 <https://doi.org/10.1016/j.jmarsys.2006.05.012>
- 950 Serreze, M. C., & Barry, R. G. (2014). The Arctic Climate System. Cambridge, UK: Cambridge
951 University Press.
- 952 Serreze, M. C., Holland, M. M., & Stroeve, J. (2007). Perspectives on the Arctic’s Shrinking
953 Sea-Ice Cover, 315(5818), 1533–1536. <https://doi.org/10.1126/science.1139426>
- 954 Soja, A. J., Tchebakova, N. M., French, N. H. F., Flannigan, M. D., Shugart, H. H., Stocks, B. J.,
955 et al. (2007). Climate-induced boreal forest change: Predictions versus current
956 observations. *Global and Planetary Change*, 56(3–4), 274–296.
957 <https://www.doi.org/10.1016/j.gloplacha.2006.07.028>
- 958 Stohl, A. (2006). Characteristics of atmospheric transport into the Arctic troposphere. *Journal of*
959 *Geophysical Research Atmospheres*, 111, D11306.
960 <https://doi.org/10.1029/2005JD006888>

- 961 Stroeve, J. C., Serreze, M. C., Holland, M. M., Kay, J. E., Malanik, J., & Barrett, A. P. (2012).
962 The Arctic's rapidly shrinking sea ice cover: a research synthesis. *Climatic Change*,
963 110(3–4), 1005–1027. <https://doi.org/10.1007/s10584-011-0101-1>
- 964 Swanson, W. F., Graham, K. A., Halfacre, J. W., Holmes, C. D., Shepson, P. B., & Simpson,
965 W. R. (2020). Arctic reactive bromine events occur in two distinct sets of environmental
966 conditions: A statistical analysis of 6 years of observations. *Journal of Geophysical*
967 *Research: Atmospheres*, 125, e2019JD032139. <https://doi.org/10.1029/2019JD032139>
- 968 Takahashi, T., Sutherland, S. C., Sweeney, C., Poisson, A., Metzl, N., Tilbrook, B., et al. (2002).
969 Global sea–air CO₂ flux based on climatological surface ocean pCO₂, and seasonal
970 biological and temperature effects. *The Southern Ocean I: Climatic Changes in the Cycle*
971 *of Carbon in the Southern Ocean*, 49(9), 1601–1622. [https://doi.org/10.1016/S0967-](https://doi.org/10.1016/S0967-0645(02)00003-6)
972 0645(02)00003-6
- 973 Takahashi, T., Sutherland, S. C., Wanninkhof, R., Sweeney, C., Feely, R. A., Chipman, D. W., et
974 al. (2009). Climatological mean and decadal change in surface ocean pCO₂, and net sea–
975 air CO₂ flux over the global oceans. *Deep-Sea Research Part II: Topical Studies in*
976 *Oceanography*, 56(8–10), 554–577. <https://doi.org/10.1016/j.dsr2.2008.12.009>
- 977 Tans, P. P., Fung, I. Y., & Takahashi, T. (1990). Observational Constraints on the Global
978 Atmospheric CO₂ Budget. *Science*, 247(4949), 1431–1438.
979 <https://doi.org/10.1126/science.247.4949.1431>
- 980 Thoning, K. W., Tans, P. P., & Komhyr, W. D. (1989). Atmospheric carbon dioxide at Mauna
981 Loa Observatory: 2. Analysis of the NOAA GMCC data, 1974–1985. *Journal of*
982 *Geophysical Research: Atmospheres*, 94(D6), 8549–8565.
983 <https://doi.org/10.1029/JD094iD06p08549>
- 984 Tremblay, J.-É., Bélanger, S., Barber, D. G., Asplin, M., Martin, J., Darnis, G., et al. (2011).
985 Climate forcing multiplies biological productivity in the coastal Arctic Ocean.
986 *Geophysical Research Letters*, 38(18). <https://doi.org/10.1029/2011GL048825>
- 987 van der Werf, G. R., Randerson, J. T., Giglio, L., van Leeuwen, T. T., Chen, Y., Rogers, B. M.,
988 et al. (2017). Global fire emissions estimates during 1997–2016. *Earth System Science*
989 *Data*, 9(2), 697–720. <https://doi.org/10.5194/essd-9-697-2017>
- 990 Verbyla, D. (2008). The Greening and Browning of Alaska Based on 1982–2003 Satellite Data.
991 *Global Ecology and Biogeography*, 17, 547–555. [https://www.doi.org/10.1111/j.1466-](https://www.doi.org/10.1111/j.1466-8238.2008.00396.x)
992 8238.2008.00396.x
- 993 Walker, D. A., Bhatt, U. S., Callaghan, T. V., Comiso, J. C., Epstein, H. E., Forbes, B. C., et al.
994 (2011). Vegetation [in Arctic Report Card 2011], [https://www.arctic.noaa.gov/Report-](https://www.arctic.noaa.gov/Report-Card)
995 Card.
- 996 Wang, Q., Jacob, D. J., Fisher, J. A., Mao, J., Leibensperger, E. M., Carouge, C. C., et al. (2011).
997 Sources of carbonaceous aerosols and deposited black carbon in the Arctic in winter-
998 spring: implications for radiative forcing. *Atmospheric Chemistry and Physics*, 11,
999 12453–12473. <https://doi.org/10.5194/acp-11-12453-2011>

- 1000 Webster, M., Gerland, S., Holland, M., Hunke, E., Kwok, R., Lecomte, O., et al. (2018). Snow in
1001 the changing sea-ice systems. *Nature Climate Change*, 8, 946–953.
1002 <https://doi.org/10.1038/s41558-018-0286-7>
- 1003 Williams, W. J., & Carmack, E. C. (2015). The ‘interior’ shelves of the Arctic Ocean: Physical
1004 oceanographic setting, climatology and effects of sea-ice retreat on cross-shelf exchange.
1005 *Progress in Oceanography*, 139, 24–41. <https://doi.org/10.1016/j.pocean.2015.07.008>
- 1006 Yasunaka, S., Murata, A., Watanabe, E., Chierici, M., Fransson, A., Heuven, S. van, et al.
1007 (2016). Mapping of the air–sea CO₂ flux in the Arctic Ocean and its adjacent seas: Basin-
1008 wide distribution and seasonal to interannual variability. *Polar Science*, 10(3), 323–334.
1009 <https://doi.org/10.1016/j.polar.2016.03.006>
- 1010 Yasunaka, S., Siswanto, E., Olsen, A., Hoppema, M., Watanabe, E., Fransson, A., et al. (2018).
1011 Arctic Ocean CO₂ uptake: an improved multiyear estimate of the air–sea CO₂ flux
1012 incorporating chlorophyll a concentrations. *Biogeosciences*, 15(6), 1643–1661.
1013 <https://doi.org/10.5194/bg-15-1643-2018>
- 1014 Zakharov, V. F. (1997). *Sea Ice in the Climate System: A Russian View* (NSIDC Special Report
1015 16). Boulder, CO, USA: National Snow and Ice Data Center. Retrieved from
1016 <https://nsidc.org/sites/nsidc.org/files/files/NSIDC-special-report-16.pdf>
- 1017 Zhao, C. L., & Tans, P. P. (2006). Estimating uncertainty of the WMO mole fraction scale for
1018 carbon dioxide in air. *Journal of Geophysical Research: Atmospheres*, 111(D8).
1019 <https://doi.org/10.1029/2005JD006003>